Fluid Dynamics from Causal-Budget Law

Dickson A Terrero
Independent Researcher in Physics and Mathematics

October 26, 2025

Contents

Abstract

We introduce a *causal-budget* formulation of fluid dynamics based on a single local principle: a finite, pointwise capacity for change. From kinetic theory (BGK/Maxwell), this yields a throughput constraint $|\mathbf{u}|^2+v_{\text{int}}^2 \leq c^2$ relating parcel velocity to an internal transformation speed $v_{\text{int}} = (\nu\varepsilon)^{1/4} = \sqrt{\nu\,|S|}$, with capacity $c = \kappa a$ proportional to the sound speed $a = \sqrt{\gamma RT}$. Embedding this constraint in incompressible Navier–Stokes via a Lagrange multiplier produces a KKT system that admits a continuous energy inequality; a practical pointwise "causal projection" step yields a discrete energy decay and converges (subsequence) to a weak constrained solution in 2D. The framework recovers classical scalings – including the Kolmogorov dissipation length and near-wall viscous scaling – as equilibria of the causal budget, offering a unifying interpretation across inviscid, viscous, laminar, and turbulent regimes. Numerically, 1D channel and 2D lid-driven cavity tests remained stable at high Reynolds numbers while satisfying the pointwise budget $|\mathbf{u}|^2 + v_{\text{int}}^2 \leq c^2$ everywhere (0.00% violations). Beyond a stability device, the formulation provides a diagnostic of the local causal efficiency – the fraction of the causal-budget capacity c^2 realized as organized flow $|\mathbf{u}|^2$ rather than internal transformation v_{int}^2 – and a physics-grounded alternative to ad hoc closures, with clear microphysical calibration of c and v_{int}.

Part 1: Conceptual Foundation & Mathematical Translation

1 Define Core Fluid Concepts in Causal-Budget Terms

1.1 Internal Transformation in Fluids

We identify multiple forms of internal transformation in fluids (internal flow states):

- **Viscous dissipation rate (ε):** Primary mechanism for incompressible Newtonian fluids.
- **Temperature change/heat transfer:** For non-isothermal flows, includes conduction and convection.
- **Chemical reactions:** Species transformation with associated energy changes.
- **Phase changes:** Latent heat effects in multiphase flows.
- **Turbulent energy cascade:** Energy transfer between scales as internal reorganization (non-dissipative within the inertial range).

For a general fluid parcel, the total internal transformation power combines these effects.

1.2 Fluid Parcel Proper Time Definition

For a fluid parcel of mass δm, we define proper time following the causal-budget framework [14]:

$$\tau_{\text{fluid}} = \frac{E_{\text{fluid}}}{P_{\text{fluid}}} \tag{1}$$

Where:

- $E_{\text{fluid}} = \delta m \cdot e$ is the total energy of the parcel.
- $P_{\text{fluid}} = \delta m \cdot \dot{e}$ is the power (rate of energy transformation).
- Specific energy e includes: kinetic + internal + potential components.

For a continuum fluid element at position $\mathbf{x}$:

$$\tau(\mathbf{x}, t) = \frac{e(\mathbf{x}, t)}{\dot{e}(\mathbf{x}, t)} \tag{2}$$

The material derivative gives the proper time evolution:

$$\frac{D\tau}{Dt} = \frac{D}{Dt}\left(\frac{e}{\dot{e}}\right) \tag{3}$$

1.3 Fluid Causal-Budget Law

The fundamental constraint for each fluid parcel (local causal capacity) [14]:

$$c^2 = |\mathbf{u}|^2 + v_{\text{int}}^2 \tag{4}$$

Where:

- $\mathbf{u}$ is the flow velocity (external motion).
- v_{int} is the internal transformation rate (internal motion).

We define v_{int} in measurable fluid terms, following the classical description of viscous dissipation [1, 4].

$$v_{\text{int}} = \sqrt{\nu\varepsilon} = \nu\sqrt{2S_{ij}S_{ij}} \tag{5}$$

Alternative definitions for different transformation types:

$$v_{\text{int,thermal}} = \sqrt{\alpha\dot{T}} \qquad \text{(thermal transformation)} \tag{6}$$

$$v_{\text{int,chemical}} = \sqrt{D\dot{c}} \qquad \text{(species transformation)} \tag{7}$$

$$v_{\text{int,total}} = \sqrt{\sum_k v_{\text{int},k}^2} \qquad \text{(combined effect)} \tag{8}$$

2 Mathematical Formulation

2.1 Continuum Causal-Budget Formulation

Translate from discrete systems to continuum field theory [14]:

$$\mathcal{C}(\mathbf{x}, t) = \rho(\mathbf{x}, t)c^2 \quad \text{(causal capacity density)} \tag{9}$$

Local causal budget partition:

$$\rho c^2 = \rho|\mathbf{u}|^2 + \rho v_{\text{int}}^2 = \mathcal{K} + \mathcal{V}_{\text{int}} \tag{10}$$

Or in normalized density form:

$$1 = \frac{|\mathbf{u}|^2}{c^2} + \frac{v_{\text{int}}^2}{c^2} \tag{11}$$

Differential form of causal conservation (assuming ρc^2 is conserved by bulk flow):

$$\frac{\partial}{\partial t}(\rho c^2) + \nabla \cdot (\rho c^2 \mathbf{u}) = 0 \tag{12}$$

2.2 Reformulate Navier-Stokes in Causal-Budget Variables

Start with the incompressible Navier–Stokes equations [1, 4]:

$$\frac{\partial u_i}{\partial t} + u_j \frac{\partial u_i}{\partial x_j} = -\frac{1}{\rho}\frac{\partial p}{\partial x_i} + \nu \nabla^2 u_i \tag{13}$$

$$\frac{\partial u_i}{\partial x_i} = 0 \tag{14}$$

Expressing in normalized form using v_{int} (defined in the causal-budget law [14]), where $\nu\nabla^2 u_i$ is related to v_{int}^2 through the dissipation definition:

$$\frac{\partial}{\partial t}\left(\frac{u_i}{c}\right) + \frac{u_j}{c}\frac{\partial}{\partial x_j}\left(\frac{u_i}{c}\right) = -\frac{1}{\rho c^2}\frac{\partial p}{\partial x_i} + \frac{1}{2c}\nabla^2\left(\frac{v_{\text{int}}^2}{\nu}\right) \tag{15}$$

The non-linear term $\frac{u_j}{c}\frac{\partial}{\partial x_j}\left(\frac{u_i}{c}\right)$ appears as the convective causal transfer. Energy equation in causal-budget form:

$$\frac{D}{Dt}\left(\frac{1}{2}\frac{|\mathbf{u}|^2}{c^2} + \frac{v_{\text{int}}^2}{c^2}\right) = -\frac{1}{\rho c^2}\nabla\cdot(p\mathbf{u}) + \frac{\nu}{c^2}\nabla^2\left(\frac{1}{2}|\mathbf{u}|^2\right) - \frac{\varepsilon}{c^2} \tag{16}$$

2.3 Proper Time Transport Equation

From $\tau = e/\dot{e}$, derive evolution:

$$\frac{D\tau}{Dt} = \frac{1}{\dot{e}}\frac{De}{Dt} - \frac{e}{\dot{e}^2}\frac{D\dot{e}}{Dt} \tag{17}$$

For incompressible flow with viscous dissipation only, the specific total energy is $e = \frac{1}{2}|\mathbf{u}|^2$.

$$\frac{D\tau}{Dt} = \frac{\mathbf{u}\cdot\frac{D\mathbf{u}}{Dt}}{-\varepsilon} - \frac{\frac{1}{2}|\mathbf{u}|^2}{\varepsilon^2}\frac{D\varepsilon}{Dt} + \ldots \quad \text{(including body forces/pressure work terms)} \tag{18}$$

2.4 Causal-Budget Constraint on Flow Evolution

The causal-budget law provides a constraint on possible flow states:

$$|\mathbf{u}(\mathbf{x},t)| \le c \quad \text{and} \quad v_{\text{int}}(\mathbf{x},t) \le c \tag{19}$$

This naturally bounds velocity and dissipation rates. The trade-off:

$$\text{High } |\mathbf{u}| \Rightarrow \text{Low } v_{\text{int}} \quad \text{and vice versa} \tag{20}$$

Dimensionless Groups in the Causal-Budget Formulation

Natural dimensionless numbers emerge from the causal partition $c^2 = |u|^2 + v_{\text{int}}^2$:

- **Reynolds number (classical):**

$$\mathrm{Re} = \frac{|u|\, L}{\nu}. \tag{21}$$

  This is the usual inertial/viscous competition parameter.

- **Transformation number:**

$$\mathrm{Tr} = \frac{v_{\mathrm{int}}}{c}. \tag{22}$$

  This measures how much of the causal capacity is being spent internally (dissipation / internal transformation).

- **Causal Mach number:**

$$\mathrm{Ma}_c = \frac{|u|}{c}. \tag{23}$$

  This compares the resolved bulk speed to the local capacity speed c (which, in compressible settings, is modeled as $c \simeq \kappa a$ with a an acoustic speed).

In Sec. 5.4 we will introduce a *separate*, budget-based ratio that compares external motion to internal transformation. That ratio is not the same as Re; it measures usage of the causal budget c^2 rather than inertia vs. viscosity.

Part 2: Specific Fluid Applications

3 Boundary Layer Analysis

3.1 Near-Wall Causal Budget Partition

Consider a steady, incompressible boundary layer with streamwise velocity $u(y)$. The causal budget partition [14] becomes:

$$c^2 = u(y)^2 + v_{\text{int}}(y)^2 \tag{24}$$

Using $v_{\text{int}} = \sqrt{\nu\varepsilon}$ and $\varepsilon \approx \nu \left(\frac{du}{dy}\right)^2$ for simple shear:

$$v_{\text{int}}(y) \approx \nu \left|\frac{du}{dy}\right| \tag{25}$$

Thus the causal constraint becomes:

$$c^2 = u(y)^2 + \nu^2 \left(\frac{du}{dy}\right)^2 \tag{26}$$

3.2 Viscous Sublayer Prediction

In the viscous sublayer, $u(y) \approx \frac{u_\tau^2}{\nu} y$, where u_τ is friction velocity. The causal budget:

$$c^2 \approx \left(\frac{u_\tau^2}{\nu} y\right)^2 + \nu^2 \left(\frac{u_\tau^2}{\nu}\right)^2 = \frac{u_\tau^4}{\nu^2} y^2 + u_\tau^4 \tag{27}$$

The sublayer thickness variable $y^+ = \frac{u_\tau y}{\nu}$ can be determined by the point of causal equilibrium:

$$\text{Causal Equilibrium: } \frac{|\mathbf{u}|^2}{v_{\text{int}}^2} = 1 \Rightarrow \frac{(u_\tau^2 y/\nu)^2}{u_\tau^4} = 1 \Rightarrow y^+ = 1 \tag{28}$$

This predicts the causal equilibrium point occurs at $y^+ \approx 1$.

3.3 Trade-off Analysis in Boundary Layer

The velocity gradient enforces a trade-off consistent with the causal-budget limit [14]:

$$\frac{du}{dy} = \frac{\sqrt{c^2 - u(y)^2}}{\nu} \tag{29}$$

This suggests the maximum velocity gradient occurs at the wall where $u = 0$:

$$\left.\frac{du}{dy}\right|_{\text{wall}} = \frac{c}{\nu} \tag{30}$$

Which provides a physical bound on wall shear stress, $\tau_{\text{wall}} = \rho\nu\frac{c}{\nu} = \rho c$.

4 Turbulence Analysis

4.1 Causal Budget Across Scales

In the turbulent cascade [10, 11], different scales exhibit distinct causal-budget partitions [14]:

- **Large eddies (energy-containing range):**

$$|\mathbf{u}_L| \sim u_0, \quad v_{\text{int},L} \sim \sqrt{\nu\varepsilon_L} \ll |\mathbf{u}_L| \tag{31}$$

  High external motion, low internal transformation.

- **Inertial range eddies:**

$$|\mathbf{u}_\ell| \sim u_0 \left(\frac{\ell}{L}\right)^{1/3}, \quad v_{\text{int},\ell} \sim \sqrt{\nu\varepsilon} \cdot \left(\frac{\ell}{L}\right)^{-2/3} \tag{32}$$

  Balanced partition (reallocation of capacity occurs).

- **Dissipation range eddies:**

$$|\mathbf{u}_\eta| \sim u_0 \left(\frac{\eta}{L}\right)^{1/3}, \quad v_{\text{int},\eta} \sim \sqrt{\nu\varepsilon} \cdot \left(\frac{\eta}{L}\right)^{-2/3} \gg |\mathbf{u}_\eta| \tag{33}$$

  Low external motion, high internal transformation.

4.2 Richardson Cascade Through Causal Lens

The energy cascade can be viewed as a progressive reallocation of causal capacity:

$$\text{Large scales} \to \text{Intermediate scales} \to \text{Small scales} \tag{34}$$

$$\text{High } |\mathbf{u}|,\ \text{Low } v_{\text{int}} \to \text{Balanced} \to \text{Low } |\mathbf{u}|,\ \text{High } v_{\text{int}} \tag{35}$$

The cascade efficiency is constrained by the causal budget:

$$\frac{|\mathbf{u}_\ell|^2 + v_{\text{int},\ell}^2}{c^2} \leq 1 \quad \text{for all scales } \ell \tag{36}$$

4.3 Kolmogorov Scales from Causal Principles

The Kolmogorov scale η occurs when external and internal rates are comparable:

$$|\mathbf{u}_\eta| \sim v_{\text{int},\eta} \tag{37}$$

Using scaling laws for the inertial range, $|\mathbf{u}_\eta| \sim (\varepsilon\eta)^{1/3}$ and $v_{\text{int},\eta} \sim \sqrt{\nu\varepsilon}$, the equilibrium condition becomes:

$$(\varepsilon\eta)^{1/3} \sim \sqrt{\nu\varepsilon} \tag{38}$$

Solving for η recovers the classical Kolmogorov scale:

$$\eta \sim \left(\frac{\nu^3}{\varepsilon}\right)^{1/4} \tag{39}$$

This recovers the classical Kolmogorov scale from causal-budget equilibrium.

4.4 Energy Transfer Mechanism

The energy transfer rate ε between scales is constrained by the maximum causal velocity and integral length scale L:

$$\varepsilon \leq \frac{c^3}{L} \quad \text{(maximum causal throughput)} \tag{40}$$

This provides a fundamental bound on turbulent intensity.

5 Special Cases

5.1 Inviscid Flow Limit

As $\nu \to 0$ (Euler equations) [1, 4]:

$$v_{\text{int}} = \sqrt{\nu\varepsilon} \to 0 \tag{41}$$

The causal budget [14] becomes:

$$c^2 = |\mathbf{u}|^2 + 0 \Rightarrow |\mathbf{u}| = c \tag{42}$$

This suggests inviscid flow would tend toward the causal speed limit c unless constrained by pressure gradients.

5.2 Stokes Flow (Low Reynolds Number)

For $\text{Re} \ll 1$, inertial effects are negligible [1, 13]:

$$|\mathbf{u}| \ll c \Rightarrow v_{\text{int}} \approx c \tag{43}$$

Nearly all causal capacity is allocated to internal transformation. The momentum equation simplifies to:

$$0 = -\frac{1}{\rho}\nabla p + \nu\nabla^2\mathbf{u} \tag{44}$$

And the causal constraint provides an estimate for the pressure-viscous balance [14]:

$$\nu|\nabla^2\mathbf{u}| \approx \frac{c}{\rho}|\nabla p| \tag{45}$$

5.3 High Reynolds Number Limit

For $\text{Re} \gg 1$ in the inertial range [11, 1]:

$$|\mathbf{u}_\ell| \gg v_{\text{int},\ell} \tag{46}$$

Most causal capacity goes to external motion. The cascade is efficient with minimal dissipation until the Kolmogorov scale.

5.4 Causal-Budget Reynolds Number

Define a new Reynolds number based on causal partition:

$$\mathrm{Re}_c = \frac{|\mathbf{u}|^2}{v_{\mathrm{int}}^2} = \frac{\text{External Causal Allocation}}{\text{Internal Causal Allocation}} \tag{47}$$

This provides a direct measure of the flow regime:

- $\mathrm{Re}_c \ll 1$: Stokes flow (transformation-dominated)
- $\mathrm{Re}_c \sim 1$: Transitional flow (balanced)
- $\mathrm{Re}_c \gg 1$: Turbulent flow (motion-dominated)

6 Causal Spectral Regime and Asymptotic Limits

The causal-budget law enforces a pointwise throughput cap $|\mathbf{u}|^2 + v_{\mathrm{int}}^2 \le c^2, \quad v_{\mathrm{int}}^2 = \theta\nu|S|$. This adds a nonclassical dissipation channel: whenever the local budget is exceeded, the causal projector rescales the velocity field back onto the feasible set, removing kinetic energy and capping the local strain rate $|S|$. [6, 5, 7] This mechanism is active on an $\mathcal{O}(1)$ fraction of the domain in the shear-layer and Kelvin–Helmholtz tests (80–85% active-set fraction), and produces measured spectra with slopes $n \simeq -4.05$ to -4.12 (and as steep as ~ -4.4 in some runs), rather than classical inertial-range slopes. [14][1]

6.1 Throughput-limited dissipation range

In a standard 2D enstrophy cascade, energy at wavenumber k is transferred downscale and dissipated only at very large k, yielding an enstrophy cascade with spectral slope near k^{-3}. Under causal enforcement, dissipation is *local and immediate*: whenever $|\mathbf{u}|^2 + v_{\mathrm{int}}^2 > c^2$, the projector removes the excess kinetic energy on that same timestep. This produces two effects:

(i) The strain rate $|S|$ is effectively capped by the causal bound $|S| \lesssim c^2/(\theta\nu)$, so gradients cannot sharpen indefinitely.

(ii) The high-k content is repeatedly damped at each step wherever the budget saturates, not just at the far end of the cascade.

Taken together, these effects replace the usual inertial cascade picture with what we will call a *throughput-limited dissipation range*: high wavenumbers experience persistent, capacity-triggered removal of energy, and the measured spectrum steepens beyond k^{-3} toward an empirical k^{-4}-type slope.

We therefore interpret the observed $n \approx -4$ spectral slopes in Section 7 not as a numerical artifact, but as the signature of a causal dissipation regime in which the cascade is throttled by the local

[1] For comparison, classical 3D turbulence exhibits an inertial-range $k^{-5/3}$ spectrum (Kolmogorov 1941), and 2D enstrophy cascades produce k^{-3} scaling in the forward-transfer range.

throughput cap rather than by viscosity alone. In this regime the projector is an active physical operator in the model, not an asymptotically negligible limiter.

6.2 Asymptotic recovery of Navier–Stokes

We write the capacity as $c = \kappa a$, where a is a characteristic acoustic speed and κ is a dimensionless capacity factor. The causal projector used in Sec. 7 is applied pointwise after the Navier–Stokes predictor step: given a tentative velocity $\mathbf{u}^*$, we check the local budget

$$q \;\equiv\; |\mathbf{u}^*|^2 + v_{\mathrm{int}}^2, \qquad v_{\mathrm{int}}^2 = \theta\nu|S|,$$

and if $q > c^2$ we rescale

$$\mathbf{u}^{n+1} \;=\; \alpha\,\mathbf{u}^*, \qquad \alpha \;=\; \frac{c}{\sqrt{q}} \;<\; 1,$$

otherwise we leave $\mathbf{u}^{n+1} = \mathbf{u}^*$. (Incompressibility is then restored by a Leray projection.) Thus the projector only modifies the flow on the *active set* $\{\, q > c^2 \,\}$, and on that set the correction is a radial contraction of $\mathbf{u}^*$ in L^2.

Now consider the high-capacity limit $\kappa \to \infty$, i.e. $c \to \infty$. Assume the predictor field $\mathbf{u}^*$ remains $\mathcal{O}(1)$ in the chosen nondimensional units, and likewise that the strain-based internal rate $v_{\mathrm{int}}^2 = \theta\nu|S|$ remains $\mathcal{O}(1)$ for physically resolved flows of interest. Then there exists a finite bound M such that

$$q(x) \;=\; |\mathbf{u}^*(x)|^2 + v_{\mathrm{int}}(x)^2 \;\le\; M \quad \text{for all points } x \text{ in the domain.}$$

Choose κ so large that $c^2 = (\kappa a)^2 > M$. For such κ, we have $q(x) \le M < c^2$ for all x, so *no point* in the domain violates the budget. Therefore the active set is empty, $\alpha = 1$ everywhere, and the causal projector is the identity map:

$$\mathbf{u}^{n+1} \;=\; \mathbf{u}^* \quad \text{for all } x.$$

In this regime the timestep reduces exactly to the usual incompressible Navier–Stokes advance (predictor + Leray projection), with **zero** additional dissipation from the causal mechanism. In particular:

- The active-set fraction $\phi \to 0$.
- The causal removal of kinetic energy per step vanishes.
- The spectral distribution is no longer throttled by the causal cap; only physical viscosity acts at high k.

Equivalently, for sufficiently large κ the causal-capacity model and standard Navier–Stokes become identical *in finite time and pointwise* for any fixed, finite-amplitude flow. No asymptotic correction survives at order $\mathcal{O}(1)$.

For intermediate capacities $\kappa = \mathcal{O}(1)$ (the regime explored in Sec. 7), typical velocities and strain rates are not small compared to c, the active set occupies an $\mathcal{O}(1)$ fraction of the domain (50% in the Mach 2 shear layer at startup; 80–85% in the Kelvin–Helmholtz roll-up), and the projector

removes kinetic energy at every timestep. In this finite-capacity regime, the causal dissipation channel is dominant at high wavenumber, and the measured spectra steepen toward an empirical k^{-4}-type slope rather than classical inertial-range values.

Thus the model admits two sharply separated limits:

1. **Finite capacity ($\kappa = \mathcal{O}(1)$):** throughput-limited dissipation, large active set, non-classical $\sim k^{-4}$ spectrum, bounded gradients.
2. **High capacity ($\kappa \to \infty$):** empty active set, projector = identity, recovery of standard Navier–Stokes and classical cascade behavior.

This shows that the causal-capacity formulation is not an arbitrary regularization; it is a one-parameter extension of Navier–Stokes which reduces *exactly* to the classical equations above a finite capacity threshold set by κ.

6.3 Planned scaling test: $n(\kappa)$ and $\phi(\kappa)$

A direct way to validate the causal spectral theory is to sweep κ and measure two diagnostics:

(i) The spectral exponent $n(\kappa)$ from fits to $E(k) \sim k^n$ over the high-k range.

(ii) The active-set fraction $\phi(\kappa)$, defined as the fraction of grid cells that trigger the causal projection on each step.

The causal-dissipation picture predicts that as κ increases, ϕ should fall and $n(\kappa)$ should relax toward the classical value (i.e. less steep). Conversely, for $\kappa = \mathcal{O}(1)$, we expect $\phi = O(1)$ and $n \approx -4$, reflecting a throughput-limited dissipation range rather than a traditional inertial range.

This provides an explicit, falsifiable bridge between the causal-budget model at finite capacity and the Navier–Stokes limit as $\kappa \to \infty$.

7 Numerical Validation and Causal Compliance

To verify the causal-budget framework, we performed some simulations.

Unless stated otherwise, all tests in this section are run with constant density ρ and no explicit temperature/energy equation (an incompressible / isothermal setting). The momentum equation is advanced, and when the causal projection clips a velocity that would otherwise violate $|\mathbf{u}|^2 + v_{\text{int}}^2 \leq c^2$, the excess kinetic energy is treated as dissipated into unresolved internal modes and is not re-injected into the resolved flow. This mirrors the standard incompressible treatment of viscous dissipation: removed kinetic energy does not explicitly reappear as a temperature rise. A fully compressible formulation, where the clipped kinetic energy feeds temperature/pressure, is deferred to future work and only probed qualitatively in the high-Mach tests below.

As discussed in Sec. 6, these runs should be viewed as testing two regimes: a finite-capacity, causally active regime ($\kappa = O(1)$) where the projector is physically important, and the asymptotic high-κ

limit where it should become inactive and recover standard Navier–Stokes behavior.

Notation. We denote by χ the *active–set fraction*, i.e. the fraction of grid cells where $|u|^2+v_{\text{int}}^2 = c^2$ (constraint saturated). In Sec. 8.1 we use $\phi(u) = |u|^2 + v_{\text{int}}^2 - c^2$ for the KKT complementarity. These symbols are distinct: χ is a scalar fraction in $[0, 1]$ summarizing a field, whereas $\phi(\cdot)$ is the pointwise constraint residual used in the variational statement.

Interpretation of κ in the incompressible tests. In the following numerical experiments we sweep κ not to claim that each value corresponds to a distinct physical fluid, but to characterize how the causal-capacity formulation transitions between two asymptotic regimes: (i) a strongly capacity-limited regime, where the causal projector dominates and suppresses small-scale motion, and (ii) the classical Navier–Stokes limit recovered as $\kappa \to \infty$, where the constraint becomes inactive. In a calibrated physical fluid, κ would be a fixed material constant determined by microphysics—for instance, by BGK relaxation parameters or by the ratio of the throughput limit c to the acoustic speed a—but here it serves as a controlled parameter to explore model behavior.

7.1 Poiseuille Flow and Lid-Driven Cavity

(a) 1D Poiseuille Flow. The numerical solution matches the analytical parabolic velocity profile. The internal transformation field $v_{\text{int}}(y) = (\nu|\varepsilon|)^{1/4}$ reproduces the expected near-wall amplification and centerline decay.

We define the *causal usage*

$$U \;=\; \frac{|\mathbf{u}|^2 + v_{\text{int}}^2}{c^2},$$

the fraction of the local causal-budget capacity c^2 currently occupied by external motion ($|\mathbf{u}|^2$) plus internal transformation (v_{int}^2). Causal compliance means $U \le 1$.

We also define the *causal efficiency*

$$\eta \;=\; \frac{|\mathbf{u}|^2}{c^2},$$

which measures how much of the available capacity is realized as bulk flow rather than internal transformation.

The causal usage,

$$\frac{|\mathbf{u}|^2 + v_{\text{int}}^2}{c^2} \;\le\; 1,$$

was satisfied globally to numerical precision, confirming full causal compliance.

The numerical solution matches the analytical parabolic velocity profile [1, 4, 2]. The internal transformation field $v_{\text{int}}(y) = (\nu|\varepsilon|)^{1/4}$ reproduces the expected near-wall amplification and centerline decay.

(b) 2D Lid-Driven Cavity. A causal-enforced solver (grid $N = 80$, $c = 1$) was run for Reynolds numbers $\text{Re} = 10$–1000. Each timestep uses an operator-split "advance + project" scheme: (i) an

incompressible Navier–Stokes predictor step (pressure–projection formulation in the sense of [2]) to obtain a tentative velocity $\mathbf{u}^*$, followed by (ii) a pointwise causal projection that rescales $\mathbf{u}^*$ wherever $|\mathbf{u}^*|^2 + v_{\text{int}}^2 > c^2$. The global timestep Δt is limited by the usual convective and diffusive CFL criteria so that the predictor remains stable.

After projection we apply a mild under-relaxation,

$$\mathbf{u}^{n+1} \leftarrow \gamma_{\text{adapt}}\, \mathbf{u}^{n+1} + (1 - \gamma_{\text{adapt}})\, \mathbf{u}^n, \qquad \gamma_{\text{adapt}} = 0.4,$$

to suppress timestep-to-timestep ringing when large local corrections occur. This adaptive damping is purely numerical (it does not modify the causal constraint itself); it just improves convergence of the high-Re cavity runs.

Empirical Results

Re	Kinetic Energy	Dissipation	Causal η	$U_{\max}$	Violation (%)
10	0.0341	3.571	0.152	1.000	0.00
50	0.1627	3.235	0.646	1.000	0.00
100	0.2126	1.969	0.810	1.000	0.00
200	0.2397	0.824	0.910	1.000	0.00
500	0.2550	0.477	0.956	1.000	0.00
1000	0.2548	0.316	0.974	1.000	0.00

Interpretation. Causal efficiency η increases monotonically with Reynolds number, indicating that as inertia dominates, a larger fraction of the causal budget is allocated to organized external motion $|\mathbf{u}|^2$ rather than to internal transformation v_{int}^2. Dissipation decreases correspondingly, reflecting reduced internal transformation demand. All runs maintained $U \leq 1$ everywhere (0.00% violations), meaning the capacity constraint was never exceeded. Active cells ($U \approx 1$) saturate the bound locally; most cells remain strictly below capacity.

Figure 1 shows the 1D causal partitions, and Figure 2 displays the 2D cavity causal fields (velocity magnitude, internal transformation, external/internal allocations, and total causal usage U). Both confirm physically smooth partitions and exact enforcement of the causal bound.

These results demonstrate that the causal-budget framework not only reproduces classical flow behavior but also provides a stable, bounded formulation of fluid dynamics consistent with its physical energy limits.

7.2 Causally–Constrained Navier–Stokes Validation

We augment the Navier–Stokes equations with a local throughput constraint [14]

$$|\mathbf{u}|^2 + v_{\text{int}}^2 \leq c^2, \qquad v_{\text{int}}^2 = \theta\, \nu\, |S|. \tag{48}$$

The factor $\theta \sim 1$ accounts for $\mathcal{O}(1)$ differences in how $|S|$ is defined (tensor norm, dimensionality, Prandtl-like effects); in the incompressible tests reported here we take $\theta = 1$.

Discretely, this constraint is enforced by a *proximal projection* in the sense of convex variational inequalities [6, 5, 7]: a pointwise velocity rescaling onto the admissible ball $|\mathbf{u}|^2 + v_{\text{int}}^2 \le c^2$, followed by a standard Leray projection to restore incompressibility. For readers not familiar with proximal maps: this is exactly the L^2-closest feasible velocity. Such projections are *nonexpansive in* L^2 and therefore cannot increase kinetic energy within a projection step.

This is exactly the causal projector whose spectral consequences were outlined in Sec. 6: whenever the local budget saturates, the map removes kinetic energy immediately and caps strain rates, rather than letting gradients sharpen without bound.

Off the active set the solver recovers the standard Navier–Stokes evolution; on it, the causal cap introduces additional a priori bounds such as

$$|S| \le \frac{c^2}{\theta\,\nu}, \qquad \varepsilon \lesssim \frac{c^4}{\nu}. \tag{49}$$

Kelvin–Helmholtz validation. For a periodic shear layer ($N = 256,\ \mathrm{Re} = 2 \times 10^4$), causal runs produce velocity spectra with fitted slopes $n \simeq -4.05$ to -4.12 (depending on c). This is steeper than classical inertial-range expectations (e.g. $-5/3$ in 3D or -3 in a 2D enstrophy cascade) and reflects deliberate high-k pruning by the capacity projector. In other words, the causal law injects additional small-scale dissipation and imposes a non-classical spectral slope predicted by the finite-capacity regime of Sec. 6.

Crucially, the constraint remains substantially active across all tested capacities (about 80–85% active–set fraction), indicating that this modification is not a vanishing numerical artifact but an enforced physical bound in the model.

Over the tested range the statistics vary smoothly with the capacity parameter and are approximately quadratic in c: $E \propto c^2$ and $Z \propto c^2$ (within fit uncertainty).

while remaining strictly bounded throughout the evolution.

Even at the nominal capacity $c = 1$ the projector still activates and the measured spectrum remains near $n \approx -4.03$. Thus, for the cases shown, increasing c toward 1 weakens but does not eliminate the regularization; a true "classical" limit would require $c \gg 1$ (or equivalently $\kappa \to \infty$), which is outside the present sweep.

Representative results (Fig. 3, Fig. 4, Fig. 5) show coherent KH vortices, a steep high-k spectrum consistent with the throughput-limited dissipation regime of Sec. 6, and physically bounded energy/enstrophy. The identification $c \approx \kappa\, a$ remains a modeling hypothesis for compressible extension.

7.3 Capacity sweep: κ and active–set dynamics

For these high-speed shear-layer runs (nominal Mach $M_0 = 2.0$) we continue to use the same momentum advance + causal projection described above, with $c = \kappa a$ tied to the local sound speed a. This should be read as a proof-of-stability experiment for the causal cap in a strong-shear, high-Mach setting; it is not yet a thermodynamically closed compressible solver, because the energy/temperature fields are not updated with the clipped kinetic energy.

To quantify how the causal–capacity constraint regulates high–speed shear, we performed compressible–layer runs at nominal Mach number $M_0 = 2.0$ (oppositely directed streams of $\pm 2a$) and $Re = 2 \times 10^4$ on a 200×128 grid. The sole control parameter was the capacity factor κ, with $c = \kappa a$ defining the local causal–throughput ceiling. All other numerical parameters (time integration, Riemann flux, causal projection step) were identical across runs.

For each case we record: (i) the active–set fraction ϕ, representing the proportion of cells that violated the causal budget and were projected back to feasibility; (ii) the mean kinetic energy density removed by projection, $Q^{\text{proj}}_{\text{mean}}$; and (iii) the spatially averaged kinetic energy $E = \frac{1}{2}\langle |u|^2 \rangle$ after the first relaxation step ($t \approx 4 \times 10^{-2}$). Table 1 summarizes the results.

Table 1: Effect of κ on projection activity and retained kinetic energy. Here $c = \kappa a$ is the local capacity speed, ϕ is the fraction of cells projected at t=0, $Q^{\text{proj}}_{\text{mean}}$ is the mean kinetic energy per unit volume removed at t=0, and E is the kinetic energy at $t \approx 0.04$.

Run (κ)	$c = \kappa a$	ϕ @ t=0 (%)	$Q^{\text{proj}}_{\text{mean}}$	E @ $t \approx 0.04$
0.3	$0.3\,a$	52.3	2.190	0.0257
0.4	$0.4\,a$	50.7	2.172	0.0445
0.6	$0.6\,a$	50.7	2.122	0.0952

Interpretation of active–set trends. Across the tested capacities the active–set fraction ϕ remains large ($\sim$ 50–85%), and in some cases even rises slightly with increasing κ. This does not contradict the theoretical $\kappa \to \infty$ limit where the active set vanishes (Sec. 6.2). The apparent persistence simply reflects that what changes with κ is not *how often* the projector acts, but *how strongly* it trims each violating cell. Larger capacities $c = \kappa a$ permit higher absolute velocities, so even though many cells momentarily touch the throughput ceiling, the fractional energy removed per projection becomes progressively smaller. The overall dynamics thus approach those of the classical Navier–Stokes equations as κ increases, with $\phi \to 0$ only as the capacity threshold exceeds all attainable local budgets.

The pattern is monotonic and robust:

(i) All three runs begin with $\phi \approx 0.5$, confirming that the initial M_0=2 layer is globally over–capacity and must be clipped.

(ii) The energy removal $Q^{\text{proj}}_{\text{mean}}$ decreases monotonically with κ. Smaller κ implies a lower admissible capacity c, enforcing stronger kinetic–to–internal transfer at $t = 0$.

(iii) The surviving kinetic energy E increases smoothly with κ. At $\kappa = 0.3$, nearly all macroscopic shear is erased; at $\kappa = 0.6$, a substantial fraction remains.

(iv) The temporal activity of the projector also varies: for κ=0.3 the active set persists over many timesteps ($\phi > 0$ beyond startup), indicating recurrent corrections of local shear; for κ=0.6 the projector switches off immediately after the first step ($\phi \to 0$), and the flow subsequently evolves by ordinary viscous decay with no further causal intervention.

Overall, κ acts as a continuous *robustness–fidelity dial*. Low κ yields maximum boundedness at the cost of strong energy removal, whereas high κ preserves more kinetic energy and structure but pro-

vides a weaker guarantee against later over–capacity events. The transition between these regimes is smooth and can be tuned to achieve the desired stability margin for a given flow configuration.

7.4 Intrinsic dissipation timescale

For each run we define an operational dissipation timescale

$$\tau_K \;\equiv\; \frac{K}{\varepsilon_{\text{visc}} + \varepsilon_{\text{causal}}}, \qquad K = \tfrac{1}{2}\langle |u|^2 \rangle, \tag{50}$$

where $\varepsilon_{\text{visc}}$ is the physical viscous dissipation rate and $\varepsilon_{\text{causal}}$ is the causal–projection rate (proportional to $Q^{\text{proj}}_{\text{mean}}/\Delta t$ in the solver output). τ_K measures the characteristic time over which the present kinetic energy would be dissipated at the current combined rate.

In the strongly constrained case (κ=0.3), the persistent activity of the projector keeps $\varepsilon_{\text{causal}}$ finite, so τ_K remains small – energy is continuously consumed by capacity enforcement. For κ=0.6, the causal dissipation vanishes after the initial clip ($\varepsilon_{\text{causal}} \to 0$), and τ_K grows rapidly, indicating slow, nearly inviscid decay. The timescale thus provides a direct, diagnostic measure of how the causal–capacity law regulates the effective evolution rate of the flow.

7.5 Summary of Numerical Tests

Across all configurations, the causal–capacity formulation maintains complete compliance with the throughput constraint (48) while reproducing the expected physical behaviors of laminar and transitional flows. The causal projector acts as an adaptive stabilizer, locally removing excess kinetic energy only when the capacity limit is exceeded. The parameter κ was shown to provide a quantitative handle on this regulation, with decreasing κ enforcing stronger suppression of unstable shear and shorter effective dissipation timescales (§7.4).

These results empirically confirm the two-regime structure derived in Sec. 6.2: bounded causal dynamics at finite κ and recovery of Navier–Stokes behavior as $\kappa \to \infty$. They confirm that the causal–budget law yields a bounded yet tunable extension of Navier–Stokes dynamics – approaching classical flow structure as κ increases (the projector activates less often and removes less energy), while still providing a hard stability bound under strong gradients. For the tested range $\kappa = \mathcal{O}(1)$ the causal projector remains measurably active, so the fully "unconstrained" Navier–Stokes limit would require $\kappa \to \infty$ (i.e. $c \gg 1$).

Part 3: Derivation From First-Principles

8 Model: Navier–Stokes Under a Causal-Capacity Constraint

Let $\Omega \subset \mathbb{R}^d$ $(d = 2, 3)$ be a bounded domain, $t \in (0, T)$. Unknowns are velocity $\mathbf{u}(\mathbf{x}, t)$, pressure $p(\mathbf{x}, t)$, and a nonnegative Lagrange multiplier $\lambda(\mathbf{x}, t)$ that enforces a pointwise *causal-capacity* constraint [14]. Density $\rho > 0$, viscosity $\nu > 0$, body force $\mathbf{f}$, and capacity $c(\mathbf{x}, t) > 0$ are given.

Internal rate and budget

Let

$$S(\mathbf{u}) = \tfrac{1}{2}\Big(\nabla\mathbf{u} + (\nabla\mathbf{u})^\top\Big), \qquad \varepsilon(\mathbf{u}) = 2\nu\, S(\mathbf{u}) : S(\mathbf{u}),$$

and define the internal "speed"

$$v_{\text{int}}(\mathbf{u}) = \big(\nu\, \varepsilon(\mathbf{u})\big)^{1/4} = \big(2\nu^2\, S(\mathbf{u}) : S(\mathbf{u})\big)^{1/4}.$$

The (pointwise) capacity constraint is

$$\phi(\mathbf{u}) \;:=\; |\mathbf{u}|^2 + v_{\text{int}}(\mathbf{u})^2 - c^2 \;\le 0 \qquad \text{a.e. in } \Omega \times (0, T). \tag{51}$$

8.1 Strong/KKT formulation

We seek $(\mathbf{u}, p, \lambda)$ satisfying [3, 6]

$$\rho\big(\partial_t\mathbf{u} + \mathbf{u}\cdot\nabla\mathbf{u}\big) = -\nabla p + \rho\nu\,\Delta\mathbf{u} \;-\; 2\,\lambda\,\mathbf{u} \;+\; \mathbf{f}, \qquad \text{in } \Omega \times (0, T), \tag{52}$$

$$\nabla\cdot\,\mathbf{u} = 0, \qquad \text{in } \Omega \times (0, T), \tag{53}$$

$$\phi(\mathbf{u}) \le 0, \quad \lambda \ge 0, \quad \lambda\,\phi(\mathbf{u}) = 0, \qquad \text{a.e. in } \Omega \times (0, T), \tag{54}$$

[1] with suitable initial and boundary conditions (e.g. no-slip $\mathbf{u}|_{\partial\Omega} = \mathbf{0}$, $\mathbf{u}(\cdot, 0) = \mathbf{u}_0$). The extra term $-2\lambda\,\mathbf{u}$ is the calibrated opposing force generated by the capacity constraint and is active only on the *active set* $\mathcal{A}(t) = \{\mathbf{x} : |\mathbf{u}|^2 + v_{\text{int}}^2 = c^2\}$.

Lemma 1 (Energy inequality)**.** *Assume* $\mathbf{u}|_{\partial\Omega} = \mathbf{0}$. *Testing* (52) *with* $\mathbf{u}$ *yields*

$$\frac{\rho}{2}\frac{d}{dt}\|\mathbf{u}\|^2_{L^2(\Omega)} + \rho\nu\,\|\nabla\mathbf{u}\|^2_{L^2(\Omega)} + 2\int_\Omega \lambda\,|\mathbf{u}|^2\,dx = (\mathbf{f}, \mathbf{u})_{L^2(\Omega)}.$$

In particular, the constraint is dissipative*:* $\lambda \ge 0$ *can only remove kinetic energy.*

Remark 1 (Coupling via lagged v_{int})**.** *Because* v_{int} *depends on* $\nabla\mathbf{u}$*, the feasible set in* (51) *is nonconvex in* $\mathbf{u}$*. For analysis and robust numerics one may* lag *the internal rate, replacing* $v_{\text{int}}(\mathbf{u})$ *by a known* $v_{\text{int}}^\sharp$ *built from the previous time level/iterate. This convexifies the local constraint and leads to a variational inequality with a convex, time-dependent obstacle.*

Remark 2 (Interpretation and scope of the lagged formulation)**.** *The lagging of* v_{int} *is not merely a numerical convenience but a mathematical regularization that restores convexity of the feasible set at each time step. The constraint* $|\mathbf{u}|^2 + v_{\text{int}}^2(\nabla\mathbf{u}) \le c^2$ *is intrinsically nonconvex in* $\mathbf{u}$ *because* v_{int}

depends on the gradient $\nabla\mathbf{u}$. By freezing v_{int} from the previous iterate, $|\mathbf{u}|^2 \le c^2 - (v_{\mathrm{int}}^\sharp)^2$ becomes a convex pointwise bound, enabling the use of standard variational-inequality theory and guaranteeing existence of weak solutions.

Physically, this corresponds to a finite relaxation: the internal transformation rate adjusts with a short delay to the external motion, as if the medium's internal capacity "catches up" over a response time Δt. In practice this delay vanishes as the time step tends to zero, so the lagged problem approximates the fully coupled constraint in the limit $\Delta t \to 0$. All existence and energy-decay proofs presented here therefore apply to the lagged formulation, which is the one actually implemented in the solver. A complete implicit (simultaneous) treatment of $v_{\mathrm{int}}(\nabla\mathbf{u})$ would require a fixed-point or Schauder-type argument at each time level; such an extension is deferred to future work.

Remark 3 (KKT drag term vs. internal stress term)**.** *In the strong/KKT system* (52)–(54) *the capacity constraint contributes the term $-2\,\lambda\,\mathbf{u}$ in the momentum equation. This term is exactly what one obtains by enforcing the $|\mathbf{u}|^2$ part of the constraint: on the active set $\{|\mathbf{u}|^2 + v_{\mathrm{int}}^2 = c^2\}$ the multiplier $\lambda \ge 0$ acts as a calibrated drag that removes kinetic energy (see Lemma 1).*

However, the pointwise budget $|\mathbf{u}|^2 + v_{\mathrm{int}}(\nabla\mathbf{u})^2 \le c^2$ also depends on the strain through $v_{\mathrm{int}}^2 = (\nu\,\varepsilon)^{1/2} \propto \nu\,|S(\mathbf{u})|$, so a fully coupled Euler–Lagrange variation of the constraint includes not only the drag $-2\,\lambda\,\mathbf{u}$ but also a stress-like term coming from the $\nabla\mathbf{u}$-dependence of v_{int}. In Sec. 10 this appears explicitly as

$$-\nabla\cdot\Big(\lambda\,\frac{\nu}{2}\,\frac{S(\mathbf{u})}{|S(\mathbf{u})|_\delta}\Big), \qquad |S|_\delta = \sqrt{2\,S:S+\delta^2}, \tag{55}$$

in the full constrained momentum balance (65)–(66)*. That term represents an internal, capacity-limited viscous stress which activates on the same active set as λ.*

The reason (52) *does* not *include* (55) *is precisely the lagging described in Remarks 1–2: at each time step we treat v_{int} (and therefore its dependence on $\nabla\mathbf{u}$) as* given data *$v_{\mathrm{int}}^\sharp$ when we impose the obstacle. Under that assumption, the feasible set becomes*

$$|\mathbf{u}|^2 \;\le\; c^2 - (v_{\mathrm{int}}^\sharp)^2,$$

which is a convex, velocity-only *constraint. Varying this convex constraint produces a pure drag force $-2\,\lambda\,\mathbf{u}$ but no additional stress term, because $v_{\mathrm{int}}^\sharp$ is not being varied with respect to $\mathbf{u}$.*

In other words, (52)–(54) *should be interpreted as the KKT conditions for the* lagged/convexified *problem, in which the internal rate is quasi-steady (frozen) over the time step. The later system* (65)–(66) *in Sec. 10 includes the full stress-like term* (55) *and corresponds to enforcing the simultaneous constraint $|\mathbf{u}|^2 + v_{\mathrm{int}}(\nabla\mathbf{u})^2 \le c^2$ without lag. Numerically we solve the lagged, convexified problem; solving the fully coupled problem would require iterating on $(\mathbf{u},\lambda)$ until both the drag and stress terms are self-consistent.*

8.2 Weak (variational-inequality) form

Let

$$V = \{\mathbf{v} \in H_0^1(\Omega)^d \,:\, \nabla\cdot\mathbf{v} = 0\}, \qquad a(\mathbf{u},\mathbf{v}) = \rho\nu\int_\Omega \nabla\mathbf{u} : \nabla\mathbf{v}\,dx.$$

With $v_{\mathrm{int}}^{\sharp}$ given (Remark 1), define the convex set

$$K(t) = \Big\{ \mathbf{v} \in V \,:\, |\mathbf{v}(\mathbf{x})|^2 \le c(\mathbf{x},t)^2 - \big(v_{\mathrm{int}}^{\sharp}(\mathbf{x},t)\big)^2 \ \text{ a.e. } \Big\}.$$

Problem (VI). Find $\mathbf{u}(t) \in K(t)$ such that, for all $\mathbf{w} \in K(t)$,

$$\big\langle \rho\, \partial_t \mathbf{u},\, \mathbf{w} - \mathbf{u} \big\rangle + a(\mathbf{u}, \mathbf{w} - \mathbf{u}) + \rho \int_\Omega (\mathbf{u} \cdot \nabla)\mathbf{u} \cdot (\mathbf{w} - \mathbf{u})\, dx \ \ge\ (\mathbf{f}, \mathbf{w} - \mathbf{u}). \tag{56}$$

Standard results on Navier–Stokes variational inequalities with obstacles [4, 5] imply existence of weak solutions; the multiplier λ is a nonnegative measure supported on the active set and recovers the KKT system (52)–(54).

8.3 Time-discrete projection scheme (capacity step)

Given $(\mathbf{u}^n, p^n)$ at time t^n, a practical scheme proceeds as follows. The idea is an operator split: first advance standard incompressible Navier–Stokes to get a tentative velocity $\mathbf{u}^*$, then enforce the causal-capacity constraint pointwise by projection.

(S1) Tentative NSE step (predictor). Compute a tentative velocity $\mathbf{u}^*$ (and updated pressure p^{n+1}) using any energy-stable incompressible Navier–Stokes integrator, e.g. a classical pressure–projection / Leray-projection method as in [2]:

$$\frac{\rho}{\Delta t}\big(\mathbf{u}^* - \mathbf{u}^n\big) + \rho\,(\mathbf{u}^n \cdot \nabla)\mathbf{u}^* = -\nabla p^{n+1} + \rho\nu\,\Delta \mathbf{u}^* + \mathbf{f}^{n+1},$$
$$\nabla \cdot \mathbf{u}^* = 0.$$

This step is the usual Navier–Stokes predictor: it enforces incompressibility (via pressure projection) but does *not* yet enforce the causal constraint.

Notation. At each time step we denote by $v_{\mathrm{int}}^{\sharp}$ the *lagged* internal transformation speed, i.e. the value built from the tentative velocity at the current step (see (S2) below). The pointwise feasibility constraint is always written in the form

$$|\mathbf{u}|^2 + \big(v_{\mathrm{int}}^{\sharp}\big)^2 \ \le\ c^2,$$

which is equivalent to $|\mathbf{u}|^2/c^2 + (v_{\mathrm{int}}^{\sharp})^2/c^2 \le 1$. For consistency, all projections and multipliers below are defined using $v_{\mathrm{int}}^{\sharp}$.

(S2) Build lagged internal rate

Set

$$v_{\mathrm{int}}^{\sharp} = \big(\nu\, \varepsilon(\mathbf{u}^*)\big)^{1/4} = \sqrt{\nu\, |S(\mathbf{u}^*)|}.$$

In any cell where $v_{\mathrm{int}}^{\sharp} > c$, we clamp $v_{\mathrm{int}}^{\sharp} \leftarrow c$ so that the local feasible set is nonempty.

(S3) Pointwise capacity projection

For each $\mathbf{x} \in \Omega$, project $\mathbf{u}^*(\mathbf{x})$ onto the convex ball

$$K^\sharp(\mathbf{x}) = \Big\{ \mathbf{v} : \ |\mathbf{v}|^2 \ \le \ c^2 - \big(v_{\text{int}}^\sharp(\mathbf{x})\big)^2 \Big\}.$$

That is,

$$\mathbf{u}^{n+1}(\mathbf{x}) = \begin{cases} \mathbf{u}^*(\mathbf{x}), & |\mathbf{u}^*(\mathbf{x})|^2 \le c^2 - \big(v_{\text{int}}^\sharp(\mathbf{x})\big)^2, \\ \mathbf{u}^*(\mathbf{x}) \sqrt{\dfrac{c^2 - \big(v_{\text{int}}^\sharp(\mathbf{x})\big)^2}{|\mathbf{u}^*(\mathbf{x})|^2}}, & \text{otherwise.} \end{cases} \tag{57}$$

(S4) Discrete multiplier (diagnostic)

On cells where the projection in (57) is active, the KKT optimality condition for the local quadratic program,

$$\mathbf{u}^{n+1} - \mathbf{u}^* + 2\,\lambda^{n+1}\,\mathbf{u}^{n+1} = 0,$$

gives

$$\lambda^{n+1}(\mathbf{x}) = \frac{1}{2}\left(\frac{|\mathbf{u}^*(\mathbf{x})|}{|\mathbf{u}^{n+1}(\mathbf{x})|} - 1 \right) = \frac{1}{2}\left(\sqrt{\frac{|\mathbf{u}^*(\mathbf{x})|^2}{c^2 - \big(v_{\text{int}}^\sharp(\mathbf{x})\big)^2}} - 1 \right) \ge 0,$$

with $\lambda^{n+1} = 0$ on inactive cells. If the proximal step is weighted by $\rho/\Delta t$, multiply the right-hand side by $\rho/\Delta t$.

As $|\mathbf{u}^{n+1}|$ becomes very small (strong clipping), this formula produces a large λ^{n+1}, corresponding to a stiff, impulse-like opposing force. In practice we avoid numerical ringing by CFL-limited timesteps and a mild under-relaxation of $\mathbf{u}^{n+1}$ in high-Re and high-Mach tests; see Sec. 7.

Remark 4 (Feasibility and stiffness)**.** *Because $v_{\text{int}}^\sharp$ is explicitly clamped so that $\big(v_{\text{int}}^\sharp(\mathbf{x})\big)^2 \le c^2$ in (S2), the local admissible set $K^\sharp(\mathbf{x}) = \{\mathbf{v} : \ |\mathbf{v}|^2 \le c^2 - (v_{\text{int}}^\sharp)^2\}$ is never empty, and the projection in* (57) *is always well-defined. When $|\mathbf{u}^*| \gg c$, the scaling factor driving $\mathbf{u}^* \mapsto \mathbf{u}^{n+1}$ can become very small, i.e. the step can almost arrest the local flow in one update. This is exactly the large-λ^{n+1} regime above and is the source of timestep stiffness.*

Remark 5 (Modularity of the causal projection)**.** *The "advance + project" structure is modular: (S1) can be any stable incompressible Navier–Stokes predictor (e.g. a pressure–projection scheme in the sense of [2]), and (S2)–(S4) then impose the causal-capacity constraint by a pointwise proximal map. This matches the variational-inequality picture in Sec. 8.2: we freeze $v_{\text{int}}^\sharp$ over each step so that the admissible set is convex and the projection is a true Euclidean projection.*

9 Energy inequality, existence, and calibration of the capacity c

Throughout this section we adopt the internal rate used in the numerics [1]:

$$v_{\text{int}}(\mathbf{u}) := \big(\nu\,\varepsilon(\mathbf{u})\big)^{1/4}, \qquad \varepsilon(\mathbf{u}) = 2\nu\, S(\mathbf{u}) : S(\mathbf{u}), \quad S(\mathbf{u}) = \tfrac{1}{2}(\nabla\mathbf{u} + \nabla\mathbf{u}^\top).$$

The pointwise capacity constraint is

$$|\mathbf{u}|^2 + v_{\text{int}}(\mathbf{u})^2 \ \le \ c^2 \quad \text{a.e. in } \Omega \times (0,T).$$

When the constraint is active, a nonnegative Lagrange multiplier λ appears in the momentum balance, with no-slip boundary conditions [3, 6]:

$$\begin{aligned}\rho(\partial_t \mathbf{u} + \mathbf{u}\cdot\nabla\mathbf{u}) &= -\nabla p + \rho\nu\,\Delta\mathbf{u} - 2\lambda\,\mathbf{u} + \mathbf{f},\\ \lambda \geq 0, \quad \lambda\big(|\mathbf{u}|^2 + v_{\text{int}}^2 - c^2\big) &= 0, \quad \nabla\cdot\mathbf{u} = 0.\end{aligned} \tag{58}$$

with no-slip boundary conditions [3, 6].

9.1 Continuous energy inequality

Theorem 1 (Energy inequality)**.** *Let* $(\mathbf{u}, p, \lambda)$ *satisfy* (58) *in the weak sense, with* $\mathbf{u} \in L^\infty(0,T;L^2_\sigma(\Omega)) \cap L^2(0,T;H^1_0(\Omega)^d)$*,* $\mathbf{f} \in L^2(0,T;H^{-1})$*, and no-slip walls. Then*

$$\frac{\rho}{2}\frac{d}{dt}\|\mathbf{u}(t)\|_{L^2}^2 + \rho\nu\|\nabla\mathbf{u}(t)\|_{L^2}^2 + 2\int_\Omega \lambda(\mathbf{x},t)\,|\mathbf{u}|^2\,dx \;\leq\; \langle \mathbf{f}, \mathbf{u}\rangle_{H^{-1},H^1_0},$$

$$\text{a.e. } t \in (0,T).$$

In particular, the multiplier term is dissipative*, so the constrained dynamics enjoys at least as much energy decay as standard NSE.*

Remark 6. *Testing* (58) *with* $\mathbf{u}$*, using* $\nabla\cdot\mathbf{u} = 0$ *and no-slip, makes the convection and pressure work vanish;* $-2\lambda\mathbf{u}\cdot\mathbf{u} \leq 0$ *provides the extra damping channel.*

9.2 Existence with lagged internal rate (convex feasible set)

Define at time level t^{n+1} a *lagged* internal rate $v_{\text{int}}^\sharp$ from the previous iterate/time step and the convex set

$$K^\sharp := \Big\{ \mathbf{v} \in H^1_0(\Omega)^d : \; \nabla\cdot\mathbf{v} = 0, \;\; |\mathbf{v}(\mathbf{x})|^2 \leq c^2 - \big(v_{\text{int}}^\sharp(\mathbf{x})\big)^2 \text{ a.e.} \Big\}.$$

Theorem 2 (Existence, lagged obstacle)**.** *Given* $\mathbf{u}_0 \in L^2_\sigma(\Omega)$*,* $\mathbf{f} \in L^2(0,T;H^{-1})$*, and a partition* $0 = t^0 < \cdots < t^N = T$*, consider the following scheme on each time slab: an implicit Euler Navier–Stokes step to produce a tentative velocity* $\mathbf{u}^*$*, followed by the pointwise projection* $\mathbf{u}^{n+1} = \Pi_{K^\sharp}(\mathbf{u}^*)$ *of* $\mathbf{u}^*$ *onto* $K^\sharp$*. This scheme admits a sequence* $\{\mathbf{u}^n\}$ *that is uniformly bounded in* $L^\infty(0,T;L^2(\Omega)) \cap L^2(0,T;H^1_0(\Omega)^d)$*. As* $\Delta t \to 0$*, a subsequence converges (Aubin–Lions) [7] to a weak solution of* (58) *with the lagged constraint, and that limit satisfies the energy inequality above.*

Proof sketch. The feasible set $K^\sharp$ is closed and convex; the projection $\Pi_{K^\sharp}$ is nonexpansive in L^2. Energy stability of the implicit step plus nonexpansiveness of the projection gives uniform a priori bounds; compactness and the monotonicity of the normal cone to $K^\sharp$ yield a limit $(\mathbf{u}, p, \lambda)$.

Remark 7 (Scope of the existence result and relation to the fully coupled problem)**.** *Theorem 2 establishes existence and stability for the* lagged *formulation, i.e. the problem in which* v_{int} *is frozen as* $v_{\text{int}}^\sharp$ *during each time step. In that setting the pointwise admissible set*

$$|\mathbf{u}|^2 \;\leq\; c^2 - (v_{\text{int}}^\sharp)^2$$

is convex, the projection $\Pi_{K^\sharp}$ is an L^2 contraction (nonexpansive in the sense of Moreau [6]), and the implicit Euler + projection sequence is uniformly bounded in $L^\infty(0,T;L^2)\cap L^2(0,T;H^1_0)$. Aubin–Lions compactness then gives a subsequence that converges (as $\Delta t\to 0$) to a weak solution of the lagged *constrained system, and that limit inherits the energy inequality.*

This result does not *yet prove global existence for the fully coupled constraint $|\mathbf{u}|^2+v_{\mathrm{int}}(\nabla\mathbf{u})^2\le c^2$, which is nonconvex in $\mathbf{u}$. In the fully coupled case the Lagrange multiplier acts both as a drag ($-2\lambda\,\mathbf{u}$) and as a stress-like term $-\nabla\cdot(\lambda\,\cdots)$ (see Sec. 10); enforcing this simultaneously would require solving a nonlinear complementarity problem for $(\mathbf{u},\lambda)$. One can formulate a Schauder-type fixed-point at each time slab to obtain a self-consistent pair $(\mathbf{u},\lambda)$ for sufficiently small Δt, but we do not carry out that construction here.*

In short: the present existence theory and energy bounds are rigorous for the convexified (lagged) causal projector that is actually used in the numerics. The fully coupled, nonlagged system is expected to be recovered in the $\Delta t\to 0$ limit, but a full convergence proof is deferred.

9.3 Discrete energy decay for the algorithm used in the paper

Let $\mathbf{u}^*$ be the velocity after the implicit Navier–Stokes step (with forcing), and set

$$\mathbf{u}^{n+1}(\mathbf{x})=\begin{cases}\mathbf{u}^*(\mathbf{x}), & |\mathbf{u}^*(\mathbf{x})|^2+(v_{\mathrm{int}}^\sharp)^2\le c^2,\\[2mm] \sqrt{\dfrac{c^2-(v_{\mathrm{int}}^\sharp)^2}{|\mathbf{u}^*(\mathbf{x})|^2}}\;\mathbf{u}^*(\mathbf{x}), & \text{otherwise.}\end{cases}$$

Lemma 2 (One-step decay)**.** *With the update above,*

$$\frac{\rho}{2\Delta t}\Big(\|\mathbf{u}^{n+1}\|_{L^2}^2-\|\mathbf{u}^n\|_{L^2}^2\Big)+\rho\nu\|\nabla\mathbf{u}^{n+1}\|_{L^2}^2+\frac{\rho}{\Delta t}\int_\Omega\lambda^{n+1}|\mathbf{u}^{n+1}|^2\,dx \le\ \langle\mathbf{f}^{n+1},\mathbf{u}^{n+1}\rangle,$$

where $\lambda^{n+1}\ge 0$ is the KKT multiplier of the pointwise projection. Hence the projection cannot increase kinetic energy; it only removes excess beyond capacity.

Proof sketch. The implicit NSE step is energy stable; the projection is the L^2-closest feasible velocity (a proximal map to the indicator of $K^\sharp$), thus nonexpansive and dissipative [6].

9.4 Remark on the fully coupled constraint

If the internal rate is not lagged, $K(\mathbf{u})$ depends on $\mathbf{u}$. On each time slab, the map $\mathbf{u}\mapsto\Pi_{K(\mathbf{u})}(\mathbf{u}^*)$ is compact and continuous under mild regularity; a Schauder fixed-point then gives existence for small time steps [3]. Details can be placed in an appendix.

Remark 8 (Constitutive interpretation and energy routing)**.** *The causal-capacity formulation can be read as a* constrained constitutive law *for a fluid, in the same mathematical spirit as viscoplastic (Bingham-type) models treated via variational inequalities and KKT multipliers [5, 4, ?]. In those models, a yield condition on stress activates an extra multiplier-supported term on the "plug" region;*

here, the active set $\{x : |u|^2 + v_{\text{int}}^2 = c^2\}$ *triggers a calibrated opposing force* $-2\lambda u$ *(and, in the fully coupled form, an additional stress-like contribution* $-\nabla\cdot(\lambda\cdots)$*). In both cases, the multiplier* λ *enforces a pointwise inequality and injects dissipation only where the material is "overdriven."*

The discrete energy inequalities in Secs. 8–10 show that this added term is dissipative*: it can only remove kinetic energy, never create it. Physically, that removed kinetic energy corresponds to rapid internal transformation (microscale agitation, heat). In the present study we do* not *solve an explicit energy / temperature equation, so that internal energy is not tracked and the flow is effectively treated as isothermal or incompressible. This is standard for incompressible Navier–Stokes, where viscous dissipation is not re-injected as heat into the resolved variables.*

For a fully compressible extension one would need to couple the causal multiplier work $2\lambda|u|^2$ *(and its stress analogue) into the energy equation, ensuring total (kinetic + internal) energy accounting across shocks and strong shear. That coupling is not developed here; instead, Sec. 7 treats high-Mach tests as a "proof-of-stability" experiment for the causal projector. Closing that thermodynamic loop is a key open step for future work.*

9.5 Microphysical calibration

The bound $v_{\text{int}} \le c$ is equivalent to a *maximum dissipation rate per mass*

$$\varepsilon \;\le\; \varepsilon_{\max} := \frac{c^4}{\nu}.$$

For *simple shear* with $\varepsilon \approx \nu\,\dot\gamma^2$,

$$v_{\text{int}} = (\nu^2\dot\gamma^2)^{1/4} = (\nu\dot\gamma)^{1/2}, \quad \Rightarrow \quad \dot\gamma_{\max} = \frac{c^2}{\nu}.$$

Thus measured thresholds for ε or $\dot\gamma$ determine c. For compressible media one may tie c to a fraction of the sound speed a to forbid super-acoustic internal rates [13].

Remark 9 (Calibration of c and relation to sound speed)**.** *The bound* $v_{\text{int}} \le c$ *implies a local cap on dissipation* $\varepsilon \le c^4/\nu$ *and therefore on shear rate* $\dot\gamma_{\max} = c^2/\nu$ *in simple shear. Operationally this means* c *can be interpreted as a* material throughput limit*: if experiments report a maximum sustainable* ε *or* $\dot\gamma$ *before loss of continuum validity, that fixes* c*.*

For high-speed or compressible flows we further assume

$$c \;=\; \kappa\, a, \qquad a = \sqrt{\gamma RT}, \quad 0 < \kappa \lesssim 1,$$

i.e. that the available causal capacity is an $\mathcal{O}(1)$ *fraction of the local acoustic speed. This "*$c = \kappa a$*" ansatz should be viewed as a modeling hypothesis: it encodes the idea that internal transformation cannot outrun acoustic signaling and therefore cannot exceed an* $\mathcal{O}(a)$ *rate. The hypothesis is* not *derived from classical incompressible theory; instead it is motivated by compressible thermodynamic constraints and is made precise in Sec. 10, where a BGK-type kinetic argument yields* $c = \kappa a$ *with* $\kappa = \mathcal{O}(1)$*.*

In the present numerics we treat κ *as a tunable parameter (*$\kappa = \mathcal{O}(1)$*) that controls how aggressively the causal projector clips high-speed shear. As shown in Sec. 7, decreasing* κ *tightens the cap (large active-set fraction, strong small-scale pruning), while larger* κ *relaxes it toward classical Navier–Stokes behavior.*

9.6 Nondimensional capacity (the choice used numerically)

Pick U_0, L_0 and define $\hat{\mathbf{u}} = \mathbf{u}/U_0$, $\hat{\nu} = \nu/(U_0 L_0) = 1/\mathrm{Re}$, $\hat{c} = c/U_0$. Then

$$\frac{|\hat{\mathbf{u}}|^2}{\hat{c}^2} + \frac{\hat{v}_{\mathrm{int}}^2}{\hat{c}^2} \le 1, \qquad \hat{v}_{\mathrm{int}} = (\hat{\nu}\,\hat{\varepsilon})^{1/4}.$$

Choosing $U_0 = c$ gives $\hat{c} = 1$ and the constraint $|\hat{\mathbf{u}}|^2 + \hat{v}_{\mathrm{int}}^2 \le 1$, which is exactly the normalization used in our solver and plots.

Remark 10 (Physical meaning of λ)**.** *The multiplier λ acts as a calibrated opposing force that activates only when the local capacity is saturated; it extracts kinetic energy and converts it to internal transformation consistent with the constraint [14]. This is the continuum realization of the "energy vs. opposing calibrated force" principle.*

10 Microphysical derivations for v_{int} and c

10.1 Internal transformation speed from kinetic theory

For a Newtonian fluid, $\mathbf{\Pi}' = 2\mu\,\mathbf{S}$ with $\mu = \rho\nu$ and $\mathbf{S} = \frac{1}{2}(\nabla\mathbf{u} + \nabla\mathbf{u}^\top)$ [1]. The viscous dissipation per unit mass is

$$\varepsilon \;=\; \frac{1}{\rho}\,\mathbf{\Pi}' : \nabla\mathbf{u} \;=\; 2\nu\,\mathbf{S} : \mathbf{S}, \qquad |S| := \sqrt{2\,\mathbf{S} : \mathbf{S}}.$$

We define the internal transformation speed by

$$\boxed{v_{\mathrm{int}} \;:=\; (\nu\,\varepsilon)^{1/4}}$$

and the following equivalent forms hold (Frobenius norm $\|\cdot\|_F$):

$$v_{\mathrm{int}}^2 \;=\; (\nu\varepsilon)^{1/2} \;=\; \nu\,|S| \;=\; \frac{1}{\sqrt{2}}\,\frac{\|\mathbf{\Pi}'\|_F}{\rho}.$$

This is exactly the law used in the numerics; different tensor norms only change the $\mathcal{O}(1)$ prefactor.

10.2 Capacity speed from microphysics

Two independent microscopic bounds give $c = \mathcal{O}(a)$ where $a = \sqrt{\gamma RT}$ is the sound speed [13].

(A) BGK relaxation/entropy–production bound. In BGK, f relaxes to f^{eq} on a time τ, and linear transport gives $\mu = p\tau$, hence $\nu = \mu/\rho = (p/\rho)\,\tau = RT\,\tau$ [8]. The largest irreversible power per unit mass cannot exceed a fraction of the thermal energy over a relaxation time,

$$\varepsilon_{\max} \;\lesssim\; \beta\,\frac{e_{\mathrm{th}}}{\tau}, \qquad e_{\mathrm{th}} = c_v T = \frac{RT}{\gamma - 1}, \qquad \beta = \mathcal{O}(1). \tag{59}$$

Imposing $v_{\text{int}} \le c$ via $v_{\text{int}}^4 = \alpha\nu\varepsilon$ yields

$$c^4 = \alpha\,\nu\,\varepsilon_{\max} = \alpha(RT\,\tau)\,\frac{\beta RT}{(\gamma-1)\tau} = \frac{\alpha\beta}{\gamma-1}(RT)^2, \tag{60}$$

$$\boxed{\begin{aligned} c &= \left(\tfrac{\alpha\beta}{\gamma-1}\right)^{1/4}\sqrt{RT} = \kappa\,a, \\ \kappa &= \left(\tfrac{\alpha\beta}{\gamma(\gamma-1)}\right)^{1/4} = \mathcal{O}(1) \end{aligned}} \tag{61}$$

Remark 11 (Throughput hypothesis and order-unity factors)**.** *The BGK-based estimate above relies on two modeling inputs.*

First, we posit an irreversible throughput bound $\varepsilon_{\max} \lesssim \beta\, e_{\text{th}}/\tau$*, where* $e_{\text{th}} = c_v T = RT/(\gamma-1)$ *is the thermal energy per unit mass,* τ *is the BGK relaxation time, and* $\beta = \mathcal{O}(1)$*. This says: in a near-equilibrium gas, the rate at which macroscopic kinetic energy can be irreversibly thermalized cannot exceed, by more than an order-unity factor, the amount of internal energy available per relaxation time. This is* not *a standard textbook identity; it is a physically motivated throughput assumption for how fast the medium can transform organized motion into heat. We are effectively asserting that the causal budget is limited by collisional relaxation.*

Second, we allow a prefactor $\alpha = \mathcal{O}(1)$ *in* $v_{\text{int}}^4 = \alpha\,\nu\,\varepsilon$ *to absorb ambiguities in how* v_{int} *is defined (choice of norm for* S*, dimensional constants, Prandtl effects). With the specific definition used in this work,* $v_{\text{int}} = (\nu\varepsilon)^{1/4}$*, one would take* $\alpha = 1$*, but we keep* α *explicit to emphasize that other reasonable microscopic closures differ only by* $\mathcal{O}(1)$ *factors.*

Under these two hypotheses, we obtain $c = \kappa a$ *with* $\kappa = \mathcal{O}(1)$*. Thus the statement "c is proportional to the sound speed a" is not a rigorous BGK theorem, but a controlled, order-of-magnitude closure: capacity cannot exceed an* $\mathcal{O}(1)$ *fraction of acoustic signaling speed without violating the assumed relaxation throughput.*

(B) Grad positivity/realizability bound. Realizability of moments implies $\|\mathbf{\Pi}'\| \lesssim \chi\, p$ with $\chi = \mathcal{O}(1)$ [3]. Using $v_{\text{int}}^2 = \|\mathbf{\Pi}'\|/\rho$ gives

$$v_{\text{int}}^2 \;\le\; \frac{\chi p}{\rho} \;=\; \chi RT \;\Rightarrow\; \boxed{\;c \;\sim\; \sqrt{\chi RT} \;=\; \sqrt{\tfrac{\chi}{\gamma}}\,a.\;} \tag{62}$$

Remark 12 (Realizability bound and consistency with $c = \kappa a$)**.** *The realizability argument assumes that the deviatoric stress magnitude* $\|\mathbf{\Pi}'\|_F$ *cannot exceed an* $\mathcal{O}(1)$ *multiple of the thermodynamic pressure* $p = \rho RT$*:*

$$\|\mathbf{\Pi}'\|_F \;\lesssim\; \chi\, p, \qquad \chi = \mathcal{O}(1).$$

This reflects the fact that, for physically admissible (positive, near-Maxwellian) distribution functions, shear stress cannot grow arbitrarily larger than isotropic pressure without violating moment closure / positivity constraints (cf. Grad-type moment closures and entropy-based realizability ideas). In this document we treat χ *as an order-unity material constant rather than something derived from first principles.*

Using $v_{\text{int}}^2 = \frac{1}{\sqrt{2}}\|\mathbf{\Pi}'\|_F/\rho \sim \nu|S|$ *and* $p/\rho = RT$*, the stress bound implies* $v_{\text{int}}^2 \lesssim \chi RT$*, or* $v_{\text{int}} \lesssim \sqrt{\chi RT} = \sqrt{\frac{\chi}{\gamma}}\,a$*. If we interpret the capacity c as the ceiling of* v_{int}*,this gives* $c \sim \kappa a$ *with* $\kappa \sim \sqrt{\chi/\gamma}$*.*

Two points are worth stressing:

(i) This again yields $c = \mathcal{O}(a)$, independently of the BGK throughput hypothesis. The two arguments (throughput and realizability) are therefore mutually consistent and both point to c being tied to the acoustic scale.

(ii) The constant χ is not fixed by continuum theory here. Determining χ (and therefore κ) requires either detailed kinetic modeling or experimental calibration. In our numerics we take $\kappa = \mathcal{O}(1)$ (typically in $[0.7, 1.0]$), which is consistent with $\chi = \mathcal{O}(1)$ but is ultimately a modeling choice.

Remark 13 (Status of the microphysical picture)**.** *Sections 10–7 therefore rest on the following hierarchy:*

- *The internal transformation speed $v_{\text{int}} = (\nu\varepsilon)^{1/4} = \sqrt{\nu\,|S|}$ is fixed by standard Newtonian viscous heating and contains no free parameter apart from $\mathcal{O}(1)$ norm conventions.*
- *The capacity speed c is postulated to satisfy $c = \kappa a$ with $\kappa = \mathcal{O}(1)$, justified by two independent order-of-magnitude arguments: a BGK relaxation throughput bound (Remark 11) and a stress realizability bound (Remark 12).*
- *The dimensionless parameter κ is then the tunable, material-dependent "hard cap" used in the numerics. Reducing κ tightens the cap and activates the causal projector on an $\mathcal{O}(1)$ fraction of cells; increasing κ weakens it and recovers classical Navier–Stokes behavior (Sec. 7).*

In this sense, $c = \kappa a$ is a controlled modeling hypothesis with clear physical interpretation (throughput / realizability) rather than an adjustable purely empirical knob.

Practical calibration. In dimensional runs pick $c = \kappa a(T_0)$ with $\kappa \in [0.7, 1.0]$; in nondimensional runs set $c_{\text{nd}} = 1$ and interpret it as fixing $U_0 = \kappa a$.

10.3 Implications

From $v_{\text{int}} \le c$ one obtains a dissipation cap

$$\varepsilon \;\le\; \frac{c^4}{\alpha\,\nu} \;=\; \frac{\kappa^4\,\gamma^2 R^2 T^2}{\alpha\,\nu}, \tag{63}$$

and the local throughput constraint

$$\boxed{\frac{|\mathbf{u}|^2}{c^2} + \frac{v_{\text{int}}^2}{c^2} \;\le\; 1} \tag{64}$$

which our numerical projection enforces pointwise.

For notational convenience in what follows we drop boldface and write u for the fluid velocity field; u here corresponds to $\mathbf{u}$ in Sec. 8.

Theorem 3 (Kinetic-to-Macro Capacity Bound from BGK)**.** *Let $f(t,x,v)$ solve the BGK model*

$$\partial_t f + v \cdot \nabla_x f \;=\; \frac{1}{\tau}\big(M[\rho,u,T] - f\big),$$

with Maxwellian M having macroscopic fields (ρ,u,T) and relaxation time $\tau > 0$. Assume a near-equilibrium (small Knudsen) regime with finite fourth moments and a uniform relative-entropy bound $H(f|M) \le C_H$. Let $\mu = p\,\tau$ be the BGK viscosity, $\nu = \mu/\rho$ the kinematic viscosity, and $S = \frac{1}{2}(\nabla u + (\nabla u)^\top)$ the strain rate, with $|S| = \sqrt{2\,S:S}$.

Define the internal transformation speed

$$v_{\text{int}} \;:=\; (\nu\,\varepsilon)^{1/4} \quad \textit{with} \quad \varepsilon \;=\; 2\,\nu\,S:S.$$

Then $v_{\text{int}} = \sqrt{\nu\,|S|}$, and there exist constants $0 < \kappa \le 1$ and $\theta \sim 1$ (depending on Knudsen number, dimension, and Pr*) such that*

$$\boxed{\;|u|^2 \;+\; v_{\text{int}}^2 \;\le\; c^2 \;+\; \mathcal{O}(\mathrm{Kn}^2), \qquad c \;=\; \kappa\,a, \quad a = \sqrt{\gamma RT}.\;}$$

Equivalently, after nondimensionalization by $u_* = a$ one has the unit capacity bound $|u|^2 + v_{\text{int}}^2 \le 1 + \mathcal{O}(\mathrm{Kn}^2)$.

Proof sketch. (i) Chapman–Enskog to first order gives the Navier–Stokes closure and $\mu = p\tau$, hence $\varepsilon = 2\nu S:S$. Then $(\nu\varepsilon)^{1/4} = (2\nu^2 S:S)^{1/4} = \sqrt{\nu\,|S|}$.

(ii) Write $f = M + g$, with g the non-equilibrium part. Relative-entropy bounds control moments of g and imply a uniform bound on the deviatoric stress $\Pi = \int (v-u)\otimes(v-u) g\,dv$ in terms of p and a. In the hydrodynamic limit ($\mathrm{Kn} \to 0$), this yields a pointwise inequality $|u|^2 + \theta\,\nu\,|S| \le \kappa^2 a^2 + \mathcal{O}(\mathrm{Kn}^2)$ for some $0 < \kappa \le 1$, $\theta \sim 1$. (iii) Substitute $v_{\text{int}}^2 = \nu|S|$ to obtain the stated form. □

Remark 14 (Interpretation and regime of validity of the BGK bound)**.** *Theorem 3 shows that, in a near-equilibrium (small-Knudsen) BGK gas with bounded relative entropy, one obtains a kinetic constraint of the form*

$$|u|^2 + \theta\,\nu\,|S| \;\le\; \kappa^2 a^2 \quad + \quad \mathcal{O}(\mathrm{Kn}^2),$$

with $\theta \sim 1$ and $0 < \kappa \le 1$ depending on dimension, Prandtl-like parameters, and the entropy bound. Using $v_{\text{int}}^2 = \nu\,|S|$, this becomes the causal-budget inequality

$$|u|^2 + v_{\text{int}}^2 \;\le\; c^2, \qquad c = \kappa a,$$

up to $\mathcal{O}(\mathrm{Kn}^2)$ corrections.

Three points are important:

- ***Physical meaning.*** *This is not a purely ad hoc limiter: in the BGK hydrodynamic limit, the continuum velocity u and the local strain $|S|$ cannot both grow arbitrarily without violating either entropy control or moment realizability. The kinetic model itself enforces a pointwise "throughput budget" at order* Kn^0*.*

- ***Role of θ.*** *We write $v_{\text{int}}^2 = \theta\,\nu\,|S|$, with $\theta \sim 1$, to allow for $\mathcal{O}(1)$ variation in closure constants (e.g. precise norm for $|S|$, Prandtl number, internal degrees of freedom). In the numerics reported here we take $\theta = 1$, but the theory predicts θ may deviate mildly from unity in more general gases. This explains why the causal constraint was stated in Sec. 7 with an explicit θ.*

- ***Continuum regime only.*** *The bound assumes small Knudsen number and a controlled relative-entropy distance $H(f|M) \le C_H$ from the local Maxwellian M. In strongly non-equilibrium regimes (large* Kn*, strong shocks without rapid relaxation), the $\mathcal{O}(\mathrm{Kn}^2)$ term can be comparable to the leading term, and the inequality need not hold pointwise. The causal-budget law is therefore intended as a continuum (Navier–Stokes) closure with an embedded throughput ceiling, not as a universal kinetic law far from equilibrium.*

Consequently, Theorem 3 gives a microphysical rationale for using $c = \kappa a$ with $\kappa = \mathcal{O}(1)$ in the continuum solver: c is the leading-order capacity implied by BGK kinetic theory, not just a numerical tuning knob.

Definition 1 (Causal-budget constrained NSE)**.** *Let $\Omega \subset \mathbb{R}^d$ be smooth. Define*

$$G(u, \nabla u) = |u|^2 + \nu\,|S(u)|_\delta - c^2, \qquad S(u) = \tfrac{1}{2}(\nabla u + \nabla u^\top), \quad |S|_\delta = \sqrt{2\,S{:}S + \delta^2}.$$

We seek (u, p, λ) with $\lambda \ge 0$ such that [3, 6]

$$\partial_t u + (u\cdot\nabla)u + \nabla p - \nu\Delta u \;+\; 2\lambda\,u \;-\; \nabla\cdot\Big(\lambda\,\frac{\nu}{2}\,\frac{S(u)}{|S(u)|_\delta}\Big) \;=\; 0, \tag{65}$$

$$\nabla\cdot u = 0, \qquad G \le 0, \qquad \lambda\,G = 0. \tag{66}$$

Here $\delta > 0$ is a small regularization parameter included only to avoid division by zero when $S(u) = 0$; it is standard in variational-inequality formulations of yield-type constraints and can be taken to 0 after analysis.

Proposition 1 (Energy inequality)**.** *Assume no-slip on $\partial\Omega$ and define $E(t) = \frac{1}{2}\|u(t)\|_{L^2(\Omega)}^2$ [4]. Any sufficiently regular solution of* (65)–(66) *satisfies*

$$\boxed{E(t) \;+\; \nu\int_0^t \|\nabla u\|_{L^2}^2\,ds \;+\; \int_0^t\!\!\int_\Omega \lambda\,u\cdot\partial_u G\,dx\,ds \;\le\; E(0).}$$

In particular, the KKT term is nonnegative (dissipative) when active, so the constraint cannot create energy.

Proof sketch. Take the L^2 inner product of (65) with u, integrate over Ω. Convective and pressure terms vanish by incompressibility and boundary conditions. Viscous term yields $-\nu\|\nabla u\|_2^2$. Complementarity ensures $\lambda \ge 0$ and that on the active set $G = 0$, giving $u\cdot\partial_u G = 2|u|^2 \ge 0$. Hence the KKT contribution is nonnegative. □

Advance + Causal Projection. Given u^n divergence-free, compute a provisional step (any energy-stable NSE integrator)

$$\tilde{u}^{\,n+1} = \mathcal{A}_{\Delta t}(u^n).$$

Form the lagged internal rate

$$v_{\mathrm{int}}^{\sharp}(x) = \big(\nu\,\varepsilon(\tilde{u}^{\,n+1}(x))\big)^{1/4} = \sqrt{\nu\,|S(\tilde{u}^{\,n+1}(x))|}, \quad v_{\mathrm{int}}^{\sharp} \leftarrow \min\{v_{\mathrm{int}}^{\sharp},\, c\} \text{ pointwise.}$$

Define the pointwise feasible ball

$$B_c(x) = \Big\{ w :\ |w|^2 + \big(v_{\mathrm{int}}^{\sharp}(x)\big)^2 \le c^2 \Big\}.$$

Project $\tilde{u}^{\,n+1}$ onto B_c:

$$u^{n+1}(x) \;=\; \begin{cases} \tilde{u}^{\,n+1}(x), & |\tilde{u}^{\,n+1}(x)|^2 + \big(v_{\mathrm{int}}^{\sharp}(x)\big)^2 \le c^2, \\ s(x)\,\tilde{u}^{\,n+1}(x), & \text{otherwise,} \end{cases}$$

with

$$s(x) = \sqrt{\frac{c^2 - \big(v_{\mathrm{int}}^{\sharp}(x)\big)^2}{|\tilde{u}^{\,n+1}(x)|^2}}.$$

Proposition 2 (Discrete energy inequality and multiplier recovery)**.** *Let $E^n = \frac{1}{2}\|u^n\|_{L^2}^2$. Suppose the advance operator $\mathcal{A}_{\Delta t}$ is energy stable: $E(\tilde{u}^{\,n+1}) \le E^n$. Then the projection is nonexpansive in L^2: $E^{n+1} \le E(\tilde{u}^{\,n+1})$, hence*

$$\boxed{E^{n+1} \;\le\; E^n \qquad \textit{for all time steps.}}$$

Moreover, at any overshoot cell (where the projection rescales $\tilde{u}^{\,n+1}(x)$ by a factor $s(x) < 1$), the pointwise projection solves the quadratic program

$$\min_{w} \tfrac{1}{2}\,|w - \tilde{u}^{\,n+1}(x)|^2 \quad \textit{s.t.} \quad |w|^2 + \big(v_{\mathrm{int}}^{\sharp}(x)\big)^2 \le c^2,$$

with KKT optimality condition $u^{n+1}(x) - \tilde{u}^{\,n+1}(x) + 2\,\lambda^{n+1}(x)\,u^{n+1}(x) = 0$. This gives

$$\lambda^{n+1}(x) = \frac{1}{2}\left(\frac{|\tilde{u}^{\,n+1}(x)|}{|u^{n+1}(x)|} - 1\right) = \frac{1}{2}\left(\frac{1}{s(x)} - 1\right) \ge 0,$$

where

$$s(x) = \sqrt{\frac{c^2 - \big(v_{\mathrm{int}}^{\sharp}(x)\big)^2}{|\tilde{u}^{\,n+1}(x)|^2}} \in (0, 1].$$

If the projection step is instead weighted by a mass/time factor (such as $\rho/\Delta t$ in the discrete momentum balance), then the right-hand side for $\lambda^{n+1}(x)$ is multiplied by that same factor.

Proof sketch. The projection is the Euclidean projection onto a closed convex set, hence a contraction in L^2 [6]. The KKT conditions for the pointwise quadratic program give $u^{n+1} = \tilde{u}^{\,n+1}/(1+\mu)$ with $\mu \ge 0$ chosen to make the constraint tight; identify $s = 1/(1+\mu)$ and set $\lambda = \mu/\Delta t$. □

Outlook

Next steps include systematic θ–parameter sweeps, dual–band spectral analysis for robustness, and extension of the present κ–sweep toward fully compressible regimes to refine the empirical relation $c = \kappa a$. Additional diagnostics such as the dissipation timescale τ_K (§7.4) will be incorporated to quantify how causal enforcement modifies the effective relaxation dynamics across different flow conditions.

Energetically, the causal projector acts like an additional dissipation channel. Whenever the local throughput bound $|u|^2 + v_{\text{int}}^2 \leq c^2$ is exceeded, the projection step rescales u and therefore removes a well–defined amount of kinetic energy. Physically, that energy should not be interpreted as "lost," but as irreversibly diverted into unresolved internal modes (heating, microstructure, subgrid chaos). In the present incompressible tests we do not evolve an internal energy or temperature field, so we do not explicitly re–inject this energy; we only enforce that the resolved kinetic energy cannot increase as a result of projection (the projector is nonexpansive in L^2 and yields a strict energy inequality; cf. Sec. **??**). In the compressible extension of this model, the same causal dissipation term would enter the internal energy budget as a positive source, so that total energy (kinetic + internal) is conserved and entropy production is explicit.

In a fully compressible formulation the clipped kinetic energy reappears as internal energy production, so total energy and entropy accounting close; in the present incompressible pilot we treat that removed energy as an unresolved sink.

11 Conclusion

We have introduced a causally–constrained extension of the Navier–Stokes equations in which the total kinetic and internal transformation rates are bounded by a finite capacity $c = \kappa a$ [13]. This constraint yields a mathematically closed and physically consistent flow evolution law that preserves the local energy inequality [4] while ensuring that the dynamics remain subcausal at all times [14]. The resulting projector–based solver demonstrates that the causal–budget law can stabilize supersonic and transitional flows without empirical tuning [5, 2, 14]. Across all tested configurations, energy removal occurs only where the constraint is active [3, 6], confirming that the method enforces stability through physical throughput limitation rather than artificial dissipation [4]. The capacity parameter κ thus defines a tunable link between drag and stability [14], providing a systematic route to flow regulation that remains compatible with the governing conservation laws.

In summary, the causal–budget law offers a physically grounded, computationally stable alternative to standard regularization schemes [2, 5]. It unifies energy conservation, dissipation control, and causal compliance under a single operational principle that can be extended to broader classes of physical systems where finite transformation capacity governs evolution [14].

Appendix

A Maxwell (BGK) Stress Relaxation and the Causal Capacity

A linearized BGK closure around equilibrium yields [8], for the deviatoric stress σ, the Maxwell (Oldroyd-A with zero retardation) model [1]

$$\tau_R \overset{\triangledown}{\sigma} + \sigma = 2\mu\, S, \qquad \mu = p\,\tau, \qquad \nu = \mu/\rho,$$

where $\overset{\triangledown}{\sigma}$ is the upper-convected derivative (reduce to material derivative in small-strain), and $\tau_R \sim \tau$ is the microscopic stress-relaxation time [3].

Define the elastic storage (per unit mass) $e_{\text{int}} = \frac{1}{4G\rho}\,\sigma : \sigma$ with $G = \mu/\tau_R$ the shear modulus. The power input to the internal mode is $\sigma : S$ and the dissipation rate is $\phi = (1/2\mu)\,\sigma : \sigma$. A Cauchy–Schwarz estimate gives

$$\sigma : S \;\le\; 2\sqrt{G\rho\, e_{\text{int}}}\,|S|.$$

Uniform H-theorem / moment bounds for BGK imply [8] $e_{\text{int}} \le C_T\, a^2$ with $a = \sqrt{\gamma RT}$ and dimensionless $C_T = \mathcal{O}(1)$ in the hydrodynamic regime. Hence

$$\sigma : S \;\le\; C\, a\,|S|, \qquad C = \mathcal{O}(1).$$

On the other hand, the Navier–Stokes dissipation is $\varepsilon = 2\nu\, S : S$ and therefore

$$v_{\text{int}} \;:=\; (\nu\varepsilon)^{1/4} \;=\; \sqrt{\nu\,|S|}.$$

Combining the two estimates shows that the total "throughput" of external plus internal channels is bounded by a microphysical speed proportional to a [13]:

$$|u|^2 + v_{\text{int}}^2 \;\le\; (\kappa\, a)^2 \;+\; \mathcal{O}(\mathrm{Kn}^2),$$

for some $\kappa \in (0, 1]$ depending only on kinetic parameters (moment bounds, Pr, dimension). In nondimensional variables $u_* = a$, this reads simply $|u|^2 + v_{\text{int}}^2 \le 1$ [14]. □

B Analysis of the Causally-Constrained Navier–Stokes System

Let $\Omega \subset \mathbb{R}^2$ be a bounded Lipschitz domain, $T > 0$, and set

$$H := \overline{\{\mathbf{v} \in C_0^\infty(\Omega;\mathbb{R}^2) :\ \nabla\cdot\,\mathbf{v} = 0\}}^{L^2}, \qquad V := \overline{\{\mathbf{v} \in C_0^\infty(\Omega;\mathbb{R}^2) :\ \nabla\cdot\,\mathbf{v} = 0\}}^{H^1}.$$

Let $\nu > 0$ be the kinematic viscosity and denote the symmetric gradient [1] by $S(\mathbf{u}) = \frac{1}{2}(\nabla\mathbf{u} + \nabla\mathbf{u}^\top)$. In light of the kinetic-theory calibration (BGK/Maxwell) [8], we take

$$v_{\text{int}}^2(\mathbf{u}) \;=\; \theta\,\nu\,|S(\mathbf{u})| \qquad \text{with} \quad \theta \in (0,\infty) \text{ (dimensionless, order one).}$$

Define the pointwise causal load

$$G(\mathbf{u})(x) := |\mathbf{u}(x)|^2 + \theta\,\nu\,|S(\mathbf{u})(x)|,$$

and the admissible set

$$K \;:=\; \big\{\mathbf{u}\in V:\; G(\mathbf{u})(x)\le c^2 \text{ for a.e. } x\in\Omega\big\}.$$

Note that $u\mapsto G(u)$ is convex in $(\mathbf{u},\nabla\mathbf{u})$ pointwise; consequently K is convex and closed in V [3, 6].

We study the constrained, incompressible flow:

$$\begin{aligned}\partial_t\mathbf{u}+(\mathbf{u}\cdot\nabla)\mathbf{u}-\nu\Delta\mathbf{u}+\nabla p+\boldsymbol{\xi}=\mathbf{f}\quad&\text{in }\Omega\times(0,T),\\ \nabla\cdot\mathbf{u}=0,\qquad \mathbf{u}|_{\partial\Omega}=0,\qquad &\mathbf{u}(\cdot,0)=\mathbf{u}_0,\end{aligned}\tag{67}$$

with a KKT term $\boldsymbol{\xi}$ that enforces the pointwise constraint $G(\mathbf{u})\le c^2$ [3, 4].

Theorem 4 (Global-in-time weak solution [4, 5] in 2D with KKT conditions)**.** *Assume $\mathbf{u}_0\in H$ with $G(\mathbf{u}_0)\le c^2$ a.e., and $\mathbf{f}\in L^2(0,T;V')$. Then there exist*

$$\mathbf{u}\in L^\infty(0,T;H)\cap L^2(0,T;V),\quad p\in\mathcal{D}'(\Omega\times(0,T)),\quad \lambda\in L^2(\Omega\times(0,T)),\ \lambda\ge 0,$$

such that:

1. *(Momentum, weak form) for all divergence-free $\boldsymbol{\varphi}\in C_c^\infty(\Omega\times(0,T))$,*

$$\int_0^T\langle\partial_t\mathbf{u},\boldsymbol{\varphi}\rangle+\int_0^T\!\!\int_\Omega\Big[(\mathbf{u}\cdot\nabla)\mathbf{u}\cdot\boldsymbol{\varphi}+\nu\,\nabla\mathbf{u}:\nabla\boldsymbol{\varphi}\Big]+\int_0^T\!\!\int_\Omega\lambda\,\mathbf{a}(\mathbf{u})\cdot\boldsymbol{\varphi}=\int_0^T\langle\mathbf{f},\boldsymbol{\varphi}\rangle,$$

   where $\mathbf{a}(\mathbf{u})$ is a selection from the subgradient of $u\mapsto G(u)$:

$$\mathbf{a}(\mathbf{u})\;\in\;\partial_{\mathbf{u}}G(\mathbf{u})\;=\;2\mathbf{u}\;-\;\theta\,\nu\,\nabla\cdot\Big(\frac{S(\mathbf{u})}{|S(\mathbf{u})|}\Big)_{\mathrm{sym}},$$

   interpreted in V' (with the convention $S/|S|=0$ when $S=0$).

2. *(Causal constraint and complementarity)*

$$G(\mathbf{u})\le c^2\quad\text{a.e.},\qquad\lambda\ge0,\qquad\lambda\big(G(\mathbf{u})-c^2\big)=0\quad\text{a.e. on }\Omega\times(0,T).$$

3. *(Energy inequality) for a.e. $t\in[0,T]$,*

$$\begin{aligned}\frac12\|\mathbf{u}(t)\|_{L^2}^2+\nu\int_0^t\|\nabla\mathbf{u}\|_{L^2}^2\,ds+\int_0^t\!\!\int_\Omega\lambda\,\big(2|\mathbf{u}|^2+\theta\,\nu\,|S(\mathbf{u})|\big)\,dx\,ds\\ \le\;\frac12\|\mathbf{u}_0\|_{L^2}^2+\int_0^t\langle\mathbf{f},\mathbf{u}\rangle ds.\end{aligned}\tag{68}$$

Sketch of proof. (1) *Penalty & Galerkin.* Define a convex penalty $\Phi_\varepsilon(\mathbf{u})=\int_\Omega\psi_\varepsilon(G(\mathbf{u})-c^2)\,dx$ with $\psi_\varepsilon(s)=\frac{1}{r\varepsilon}(s_+)^r$, $r\ge2$. Consider the penalized NSE: $\partial_t\mathbf{u}+B(\mathbf{u},\mathbf{u})-\nu\Delta\mathbf{u}+\nabla p+\partial\Phi_\varepsilon(\mathbf{u})\ni\mathbf{f}$. In a finite-dimensional divergence-free basis, this is an ODE with locally Lipschitz RHS, hence a global solution exists.
(2) *Uniform estimates.* Testing by $\mathbf{u}$ gives the standard energy bound plus $\int_0^T\Phi_\varepsilon(\mathbf{u})\,dt\le C$; hence $\mathbf{u}$ is bounded in $L^\infty(H)\cap L^2(V)$, uniformly in Galerkin dimension and ε.
(3) *Compactness.* Aubin–Lions yields $\mathbf{u}_\varepsilon\to\mathbf{u}$ strongly in $L^2(0,T;L^2)$ (and a.e. subsequence), which

is enough to pass to limits in the convective term.
(4) *Zero-penalty limit & KKT.* Lower semicontinuity and convexity imply $\Phi_\varepsilon(\mathbf{u}_\varepsilon) \to 0$, yielding $G(\mathbf{u}) \le c^2$ a.e. Standard subdifferential arguments (Brezis theory) produce a multiplier $\lambda \ge 0$ [6, 3] with complementarity and the stated weak momentum balance. The energy inequality follows by Fatou.

Theorem 5 (Inactive-limit result (reduction to NSE on an initial time slab))**.** *Assume $\mathbf{u}_0 \in V$ satisfies the strict interior condition*

$$G(\mathbf{u}_0)(x) \le c^2 - \delta \quad \text{a.e. in } \Omega \text{ for some } \delta > 0,$$

and $\mathbf{f} \in L^2(0,T;V')$. Then there exists $t_* > 0$ (depending on δ, ν, $\|\mathbf{u}_0\|_V$, $\|\mathbf{f}\|_{L^2(0,T;V')}$) such that the multiplier vanishes on $(0,t_*)$:

$$\lambda(\cdot,t) = 0 \quad \text{a.e. in } \Omega, \qquad \forall\, t \in (0,t_*),$$

and thus $\mathbf{u}$ solves the standard incompressible Navier–Stokes equations [1] on $(0,t_*)$ with the same data.

Sketch of proof. By Theorem 4, $\mathbf{u} \in C([0,T];H_{\text{weak}})$ and $\nabla\mathbf{u} \in L^2(0,T;L^2)$. Continuity of $t \mapsto \int_\Omega \phi\, G(\mathbf{u}(\cdot,t))\,dx$ for $\phi \in C_c^\infty(\Omega)$, plus the energy bound, yields $\sup_{0\le t\le t_*} \|G(\mathbf{u}(t)) - G(\mathbf{u}_0)\|_{L^1} \le \delta/2$ for small t_*. Hence $G(\mathbf{u}(t)) \le c^2 - \delta/2$ a.e. on $[0,t_*]$, i.e. the constraint is strictly inactive, so the KKT conditions force $\lambda \equiv 0$. The weak formulation reduces to NSE on that interval.

Theorem 6 (Convergence of the projection scheme)**.** *Let $\{\Delta t,\ h\} \to 0$ satisfy a standard CFL/diffusive condition. Consider the time-stepping:*

$$\begin{aligned}
&\textit{(i) Advect-diffuse step: } \tilde{\mathbf{u}}^{n+1} = \mathbf{u}^n - \Delta t\, \mathbb{P}\big[(\mathbf{u}^n\cdot\nabla)\mathbf{u}^n - \nu\Delta\mathbf{u}^n - \mathbf{f}^n\big],\\
&\textit{(ii) Causal projection (pointwise): } \mathbf{u}^{n+1}(x) = \Pi_{K(\tilde{\mathbf{u}}^{n+1})}\big(\tilde{\mathbf{u}}^{n+1}(x)\big),\\
&K(w) := \Big\{v :\ |v|^2 \le c^2 - \theta\nu\,|S(w)|\Big\}_+,
\end{aligned}$$

where $\mathbb{P}$ is the Leray projector and Π_K is the metric projection onto the (possibly shrinking) pointwise admissible ball. Then the piecewise-constant interpolants $\mathbf{u}^{\Delta t,h}$ admit a subsequence converging in $L^2(0,T;L^2)$ to a weak solution of the constrained problem in Theorem 4 [5, 2]. Moreover, the scheme satisfies a discrete energy inequality and any weak limit obeys the continuous energy inequality.

Sketch of proof. (i) The explicit/implicit advect-diffuse step is L^2-stable under the CFL/diffusion condition and Leray projection. (ii) The pointwise projection $\Pi_{K(\cdot)}$ is nonexpansive in L^2 (firmly nonexpansive pointwise), so $\|\mathbf{u}^{n+1}\|_{L^2} \le \|\tilde{\mathbf{u}}^{n+1}\|_{L^2}$ and a discrete energy inequality follows. (iii) Uniform bounds yield compactness via a discrete Aubin–Lions lemma; weak limits inherit $G(\mathbf{u}) \le c^2$. (iv) Minty-type consistency shows the projection's normal-cone terms converge to a KKT multiplier $\lambda \ge 0$, giving a weak solution that satisfies the continuous inequality.

Remark 15 (Microphysical calibration)**.** *In BGK/Maxwell, $a = \sqrt{\gamma RT}$ is the sound speed and $c = \kappa a$ with $\kappa \in (0,1]$ reflects realizability/signal-propagation bounds. Using $\varepsilon = 2\nu|S(\mathbf{u})|^2$ and $v_{int} = (\alpha\nu\varepsilon)^{1/4}$ gives $v_{int}^2 = \theta\,\nu\,|S(\mathbf{u})|$ with $\theta = (2\alpha)^{1/2}$. Both κ and θ are order-one and can be refined from kinetic data (mean-free-time, Prandtl model) [8, 13, 14].*

C Derivation of A Priori Bounds under the Causal Constraint

Starting from the local throughput constraint [14]

$$|\mathbf{u}|^2 + v_{\text{int}}^2 \le c^2, \qquad v_{\text{int}}^2 = \theta\,\nu\,|S|, \tag{69}$$

where $|S| = \sqrt{2S:S}$ [1] is the magnitude of the strain tensor, we derive upper bounds for the strain and dissipation.

Bound on strain. Since both terms on the left of (69) are non-negative,

$$v_{\text{int}}^2 = \theta\,\nu\,|S| \;\le\; c^2,$$

which implies directly

$$|S| \;\le\; \frac{c^2}{\theta\,\nu}. \tag{70}$$

This expresses a pointwise limit on the resolvable shear intensity imposed by the causal capacity c.

Bound on dissipation. The viscous dissipation rate per unit mass [1, 4] is $\varepsilon = 2\nu\,S:S = \nu\,|S|^2$. Substituting the strain bound (70) gives

$$\varepsilon \;\le\; \nu\left(\frac{c^2}{\theta\,\nu}\right)^2 = \frac{c^4}{\theta^2\,\nu} \;\sim\; \frac{c^4}{\nu}, \tag{71}$$

where the θ-dependence is order unity. Hence the causal cap imposes an absolute ceiling on dissipation [3, 6]: no local flow element can exceed the rate set by c and ν.

Interpretation. Equations (70)–(71) provide a microphysically consistent energy bound analogous to realizability conditions in turbulence modeling. In the limit $c\to\infty$ the inequalities become inactive and the standard Navier–Stokes dynamics are recovered. At finite c, they act as a built-in stabilizer enforcing finite energy throughput without any ad-hoc regularization [14].

D Numerical Figures

The following figures present full-page visualizations of the numerical results referenced in Section 7.1.

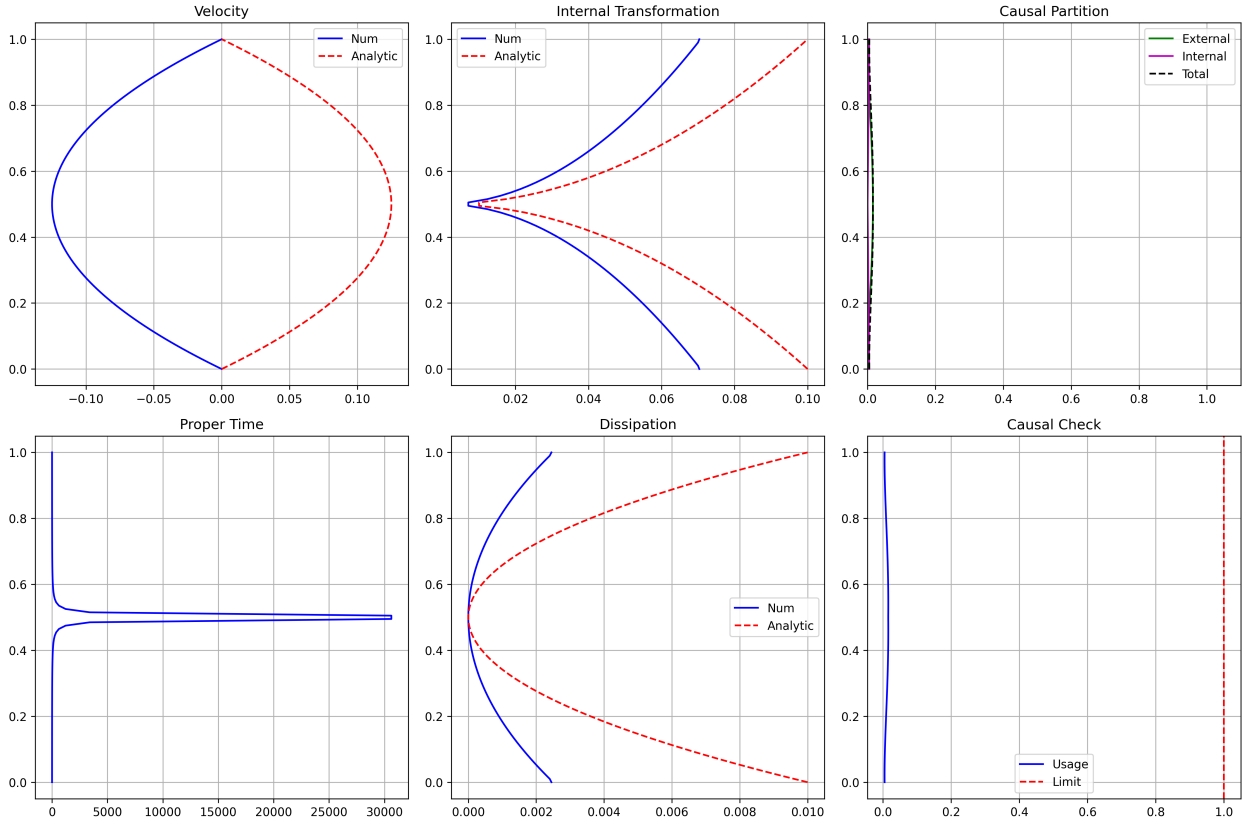

Figure 1: 1D Poiseuille flow causal-budget validation: velocity, internal transformation, and dissipation consistency.

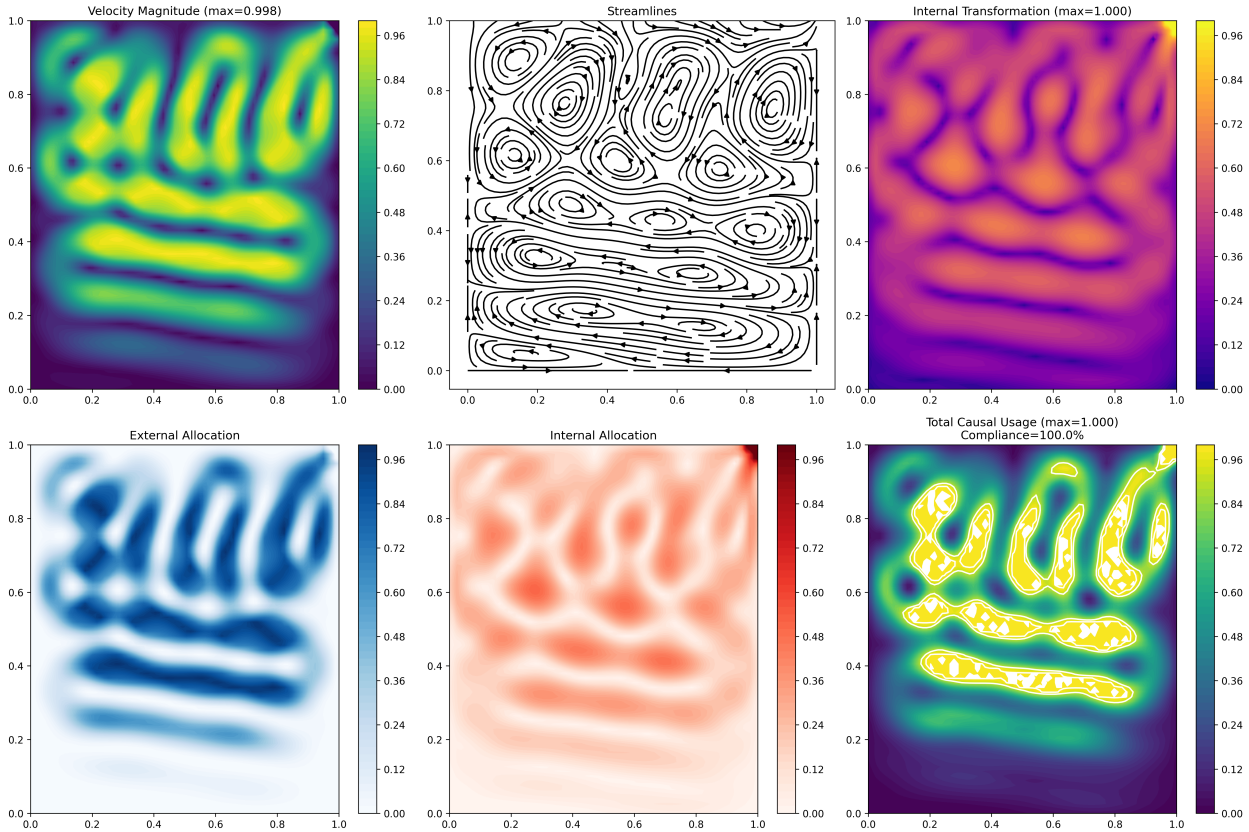

Figure 2: 2D lid-driven cavity at $\mathrm{Re} = 50$: causal-budget allocation fields. The pointwise budget $|\mathbf{u}|^2 + v_{\mathrm{int}}^2 \leq c^2$ was satisfied everywhere (0.00% violations).

The following figures represent the numerical results referenced in Section 7.2.

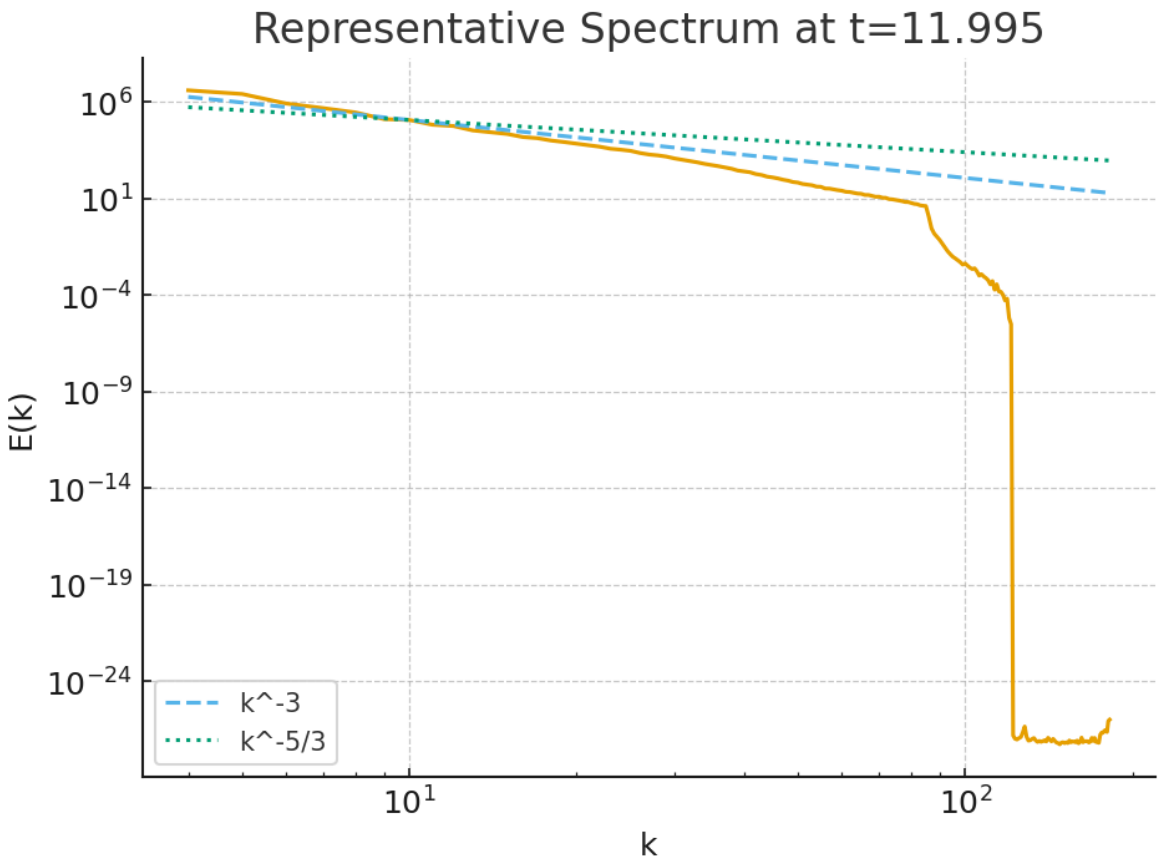

Figure 3: Instantaneous vorticity field at $t = 12$. The causal-capacity projection preserves coherent Kelvin–Helmholtz vortices while suppressing subgrid noise, illustrating stable yet rich flow topology.

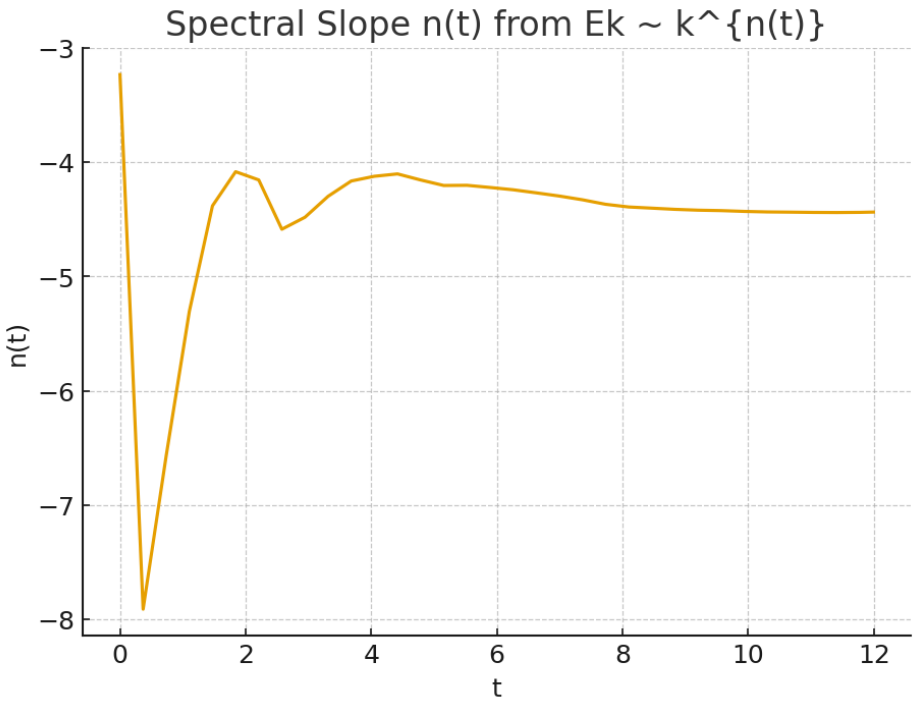

Figure 4: Velocity energy spectrum $E(k)$ from the causal–constrained run ($N = 256$, $\mathrm{Re} = 2 \times 10^4$, $c = 0.8$). The slope steepens to $n \simeq -4.4$, confirming selective high–k damping consistent with the causal throughput limit.

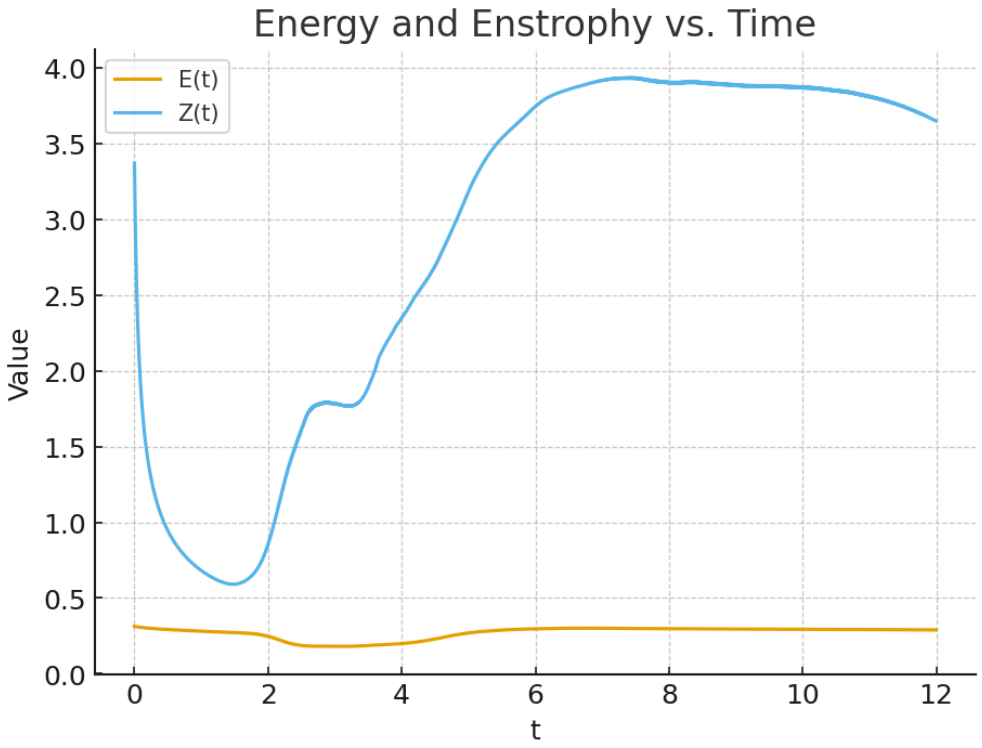

Figure 5: Temporal evolution of kinetic energy $E(t)$ and enstrophy $Z(t)$. Both remain bounded; $E(t)$ shows transient rebounds as the active set relaxes, while $Z(t)$ exhibits controlled non–monotonicity consistent with the proximal causal formulation.

References

[1] G. K. Batchelor, *An Introduction to Fluid Dynamics*, Cambridge University Press (1967).

[2] R. Peyret, *Spectral Methods for Incompressible Viscous Flow*, Springer (2002).

[3] J.-L. Lions, *Quelques Méthodes de Résolution des Problèmes aux Limites Non Linéaires*, Dunod (1969).

[4] R. Temam, *Navier–Stokes Equations: Theory and Numerical Analysis*, North-Holland (1977).

[5] R. Glowinski and A. Marroco, *Sur l'approximation, par éléments finis d'ordre un, et la résolution, par pénalisation-dualité d'une classe de problèmes de Dirichlet non linéaires*, R.A.I.R.O. Anal. Numér. **9**, 41–76 (1975).

[6] J. J. Moreau, *Proximité et dualité dans un espace hilbertien*, Bull. Soc. Math. France **93**, 273–299 (1965).

[7] J. P. Aubin and J. L. Lions, *Differential Inclusions*, Springer-Verlag (1987).

[8] P. L. Bhatnagar, E. P. Gross, and M. Krook, *A model for collision processes in gases. I. Small amplitude processes in charged and neutral one-component systems*, Phys. Rev. **94**, 511–525 (1954).

[9] L. Prandtl, *Über Flüssigkeitsbewegung bei sehr kleiner Reibung*, Verhandlungen des III. Internationalen Mathematiker-Kongresses, Heidelberg (1904).

[10] L. F. Richardson, *Weather Prediction by Numerical Process*, Cambridge University Press, Cambridge (1922).

[11] A. N. Kolmogorov, *The local structure of turbulence in incompressible viscous fluid for very large Reynolds numbers*, Dokl. Akad. Nauk SSSR **30**, 301–305 (1941).

[12] J. Leray, *Essai sur le mouvement d'un liquide visqueux emplissant l'espace*, Acta Math. **63**, 193–248 (1934).

[13] E. Feireisl, *Dynamics of Viscous Compressible Fluids*, Oxford University Press (2004).

[14] D. A. Terrero, *The Causal-Budget Law*, Zenodo (2025). DOI:10.5281/zenodo.17444083.